Systematic Review

Recent Advances in Carbon-Based Sensors for Food and Medical Packaging Under Transit: A Focus on Humidity, Temperature, Mechanical, and Multifunctional Sensing Technologies—A Systematic Review

Siting Guo [1], Iza Radecka [2,*], Ahmed M. Eissa [2], Evgeni Ivanov [3,4], Zlatka Stoeva [5] and Fideline Tchuenbou-Magaia [1,*]

[1] Centre for Engineering Innovation and Research, School of Engineering, Computing and Mathematical Sciences, Faculty of Science and Engineering, University of Wolverhampton, Wolverhampton WV1 1LY, UK; s.guo3@wlv.ac.uk

[2] Research Institute of Healthcare Sciences, School of Pharmacy & Life Sciences, Faculty of Science and Engineering, University of Wolverhampton, Wulfruna Street, Wolverhampton WV1 1LY, UK; a.m.eissa@wlv.ac.uk

[3] Open Laboratory on Experimental Micro and Nano Mechanics (OLEM), Institute of Mechanics, Bulgarian Academy of Sciences, Acad. G. Bonchev Str. Block 4, 1113 Sofia, Bulgaria; ivanov_evgeni@imbm.bas.bg

[4] Research and Development of Nanomaterials and Nanotechnologies—NanoTech Lab Ltd., Acad. G. Bonchev Str. Block 4, 1113 Sofia, Bulgaria

[5] DZP Technologies Limited, Cambridge CB4 2HY, UK

[*] Correspondence: i.radecka@wlv.ac.uk (I.R.); f.tchuenbou-magaia@wlv.ac.uk (F.T.-M.)

Abstract: All carbon-based sensors play a critical role in ensuring the sustainability of smart packaging while enabling real-time monitoring of parameters such as humidity, temperature, pressure, and strain during transit. This systematic review covers the literature between 2013 and 16 November 2024 in the Scopus, Web of Science, IEEE Xplore, and Wiley databases, focusing on carbon-based sensor materials, structural design, and fabrication technologies that contribute to maximizing the sensor performance and scalability with particular emphasis on food and pharmaceutical product packaging applications. After being subjected to the inclusion and exclusion criteria, 164 studies were included in this review. The results show that most humidity sensors are made using graphene oxide (GO), though there is some progress toward cellulose and cellulose-based materials. Graphene and carbon nanotubes (CNTs) are predominant in temperature and mechanical sensors. The application of composites with structural design (e.g., porous and 3D structures) significantly improves sensitivity, long-term stability, and multifunctionality, whereas manufacturing methods such as spray coating and 3D printing further drive production scalability. The transition from metal to carbon-based electrodes could also reduce the cost. However, the scalability, long-term stability, and real-world validation remain challenges to be addressed. Future research should further enhance the performance and scalability of carbon-based sensors through low-energy fabrication techniques and the development of sustainable advanced materials to provide solutions for practical applications in dynamic transportation environments.

Keywords: carbon-based sensors; humidity sensors; temperature sensors; mechanical sensors; multifunctional sensors; smart food packaging; smart pharmaceutical product packaging; real-time monitoring

1. Introduction

The rapid expansion of global trade and online shopping is coupled with an increased challenge in maintaining product quality, safety, and integrity during storage and transportation. Packaging plays an important role in maintaining product characteristics, especially for food and medical or pharmaceutical products, which are susceptible to contamination, degradation, spoilage, and physical damage leading to health risks, economic losses, and environmental impacts [1–4]. Indeed, GBP 14 billion of food is wasted annually in the UK [5], and the UK Health Security Agency, UKHSA (2022), reported GBP 5.7 million worth of vaccines wasted in 2019 and that 76% of these losses could have been prevented with better control of logistics, transportation, and storage conditions. At a global level, an estimated 1.3 billion tons of food are wasted throughout the food supply chain [6]. This waste corresponds to approximately 3.3 gigatons of CO_2 equivalent emissions each year [7], accounting for 8–10% of total global greenhouse gas emissions [2]. If it were considered as a country, food waste would represent the third biggest source of these emissions worldwide [6]. These statistics underscore the urgent need for advanced packaging solutions to ensure product safety, minimize waste, and promote sustainability. This need is already exemplified by the expected smart packaging market growth from USD 23.33 billion in 2023 to USD 40.02 billion by 2032 [8], with food/beverages having the largest market share (34.6% share) when compared to other segments (Figure 1).
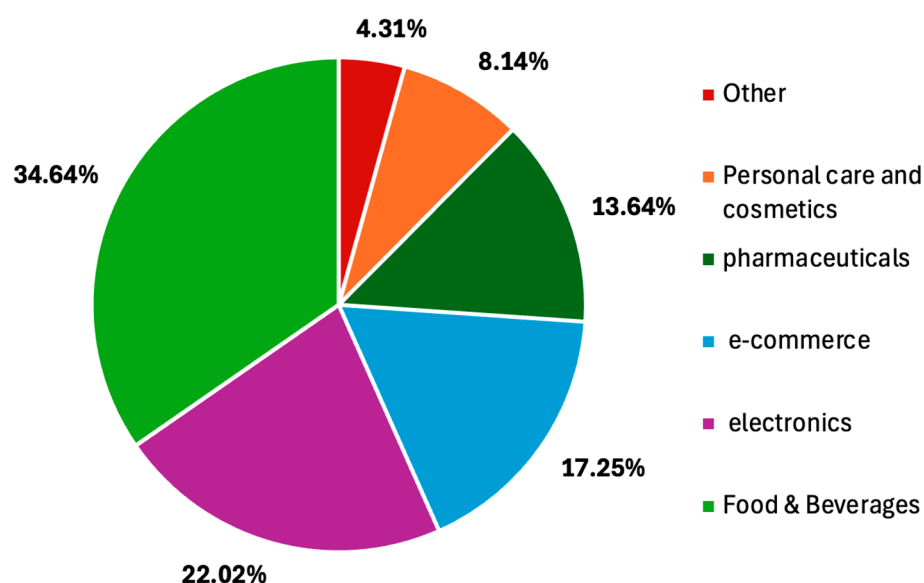
Figure 1. Global smart packaging market share 2023 (adapted from Fortune business insights, 2024) [8].

Smart packaging encompasses a range of technologies that integrate embedded sensors, identifiers, and various tools to enhance products safety, efficiency, sustainability, traceability, and user experience. This includes intelligent packaging, which monitors and communicates information about the product quality and state [9], and connected packaging through the Internet of Things and cloud systems [10]. This review focuses on sensors, which allow the monitoring and response of smart packaging to the dynamic transportation environments, where products are exposed to various fluctuating conditions such as humidity, temperature, and mechanical stress, thereby compromising their quality, safety, and integrity.

Packaging for food and medical/pharmaceutical products is designed to accommodate different internal pressures based on the packaging type, such as vacuum-seal packaging (0.1–100 kPa) [11], modified atmosphere packaging (5–50 kPa) [12], flexible or semi-rigid

packaging (0.1–50 kPa) [13], and bulk packaging (1–500 kPa) [14]. Additionally, packaging is likely to encounter various mechanical stresses, including vibrations, compression and impacts from drops during storage, handling, and transportation (Table 1). These mechanical stresses can be monitored using mainly pressure and strain sensors. Pressure sensors measure the force per unit area of the material, helping to detect internal pressure changes to identify product leakage, packaging sealing damage, or defects, such as in blisters incomplete sealing and delamination. They also monitor external forces for preventing bursts and supporting the monitoring of packaging integrity under transportation stresses such as stacking, handling, and impacts. Conversely, strain sensors detect the deformation of the material [15] and can find applications in detecting cracks, fatigue, or tears that may jeopardize the packaging barrier properties and compromise the product safety, quality, and economical value.

Table 1. Sensing range and storage conditions for the safe transportation of food and medical/pharmaceutical products.

Category	Condition	Type	Range	Reference
Humidity	-	Dried food	10–65%RH	[16]
	Cold chain	Perishable food	75–95%RH	[17]
	Ambient	Pharmaceuticals	<60%RH	[18]
Temperature	Frozen	Food	−40−−18 °C	[19]
		Medical	−40−−18 °C	[19]
	Cold chain	Food	0–4 °C	[19]
		Medical	2–8 °C	[20]
	Chilled	Food	4–8 °C	[19]
		Medical	5–25 °C	[21]
	Ambient	Food	8–40 °C	[21]
		Medical	15–25 °C	[18]
Mechanical stress	Compression	Pressure	34–344 kPa	[22]
		Strain	1–15%	
	Impact/shock	Pressure	5–40 G	[23]
		Strain	1–10%	
	Vibration	Pressure	3–200 Hz	[24]
		Strain	0.1–2% over time	

Humidity sensors play vital roles in maintaining optimal moisture levels, issuing real-time alerts to prevent microbial growth and dehydration that could compromise product texture, potency, or freshness. Similarly, temperature sensors monitor thermal conditions, providing immediate feedback to prevent spoilage, protein denaturation, loss of functionality, and degradation. Multifunctional sensors integrate multiple detection capabilities, such as humidity, temperature, and mechanical sensing, into single platforms.

While acknowledging the key role of smart packaging in ensuring products quality and safety during transportation, reducing waste, extending shelf life and improving supply chain management [10], their general adoption is hindered by challenges related to cost, scalability, and environmental sustainability.

Recent advancements in sensor technology, particularly using carbon-based materials, offer a pathway to overcoming these challenges. These materials including graphene (G), graphene oxide (GO), reduced graphene oxide (rGO), carbon nanotubes (CNTs), carbon

nanohorns (CNHs), graphene quantum dots (GQDs), and carbon black (CB), which exhibit exceptional properties, such as high electrical conductivity, mechanical strength and flexibility, thermal stability, light weight, and large surface area [25]. These properties enable enhanced sensing performance, miniaturization, and adaptability to diverse stimuli, including humidity, temperature, pressure, strain, and volatile organic compounds (VOCs). In addition, carbon-based materials are generally more cost-effective and relatively environmentally friendly compared to traditional high-performance materials such as silver [26]. However, certain high-purity carbon-based material production processes, particularly chemical vapor deposition (CVD), involve metal catalysts (nickel, iron, cobalt) which may cause heavy metal contamination due to residual catalyst particles [27]. Effective purification methods, including acid treatments, oxidation, thermal annealing, and magnetic separation, as well as employing low-toxicity or metal-free catalysts, have been developed to remove residual metal catalysts from carbon-based materials [27,28]. Technologies proposing catalyst-free synthesis include mechanical exfoliation, liquid-phase exfoliation, electrochemical exfoliation, Hummers' process, plasma-enhanced catalyst-free CVD, and laser-induced methods [28–31] or the use of biomass-derived carbons sources [32], thus, offering environmentally friendly options. These technologies nevertheless still face challenges regarding mass production and production efficiency. To fully harness the environmental and economic potential of carbon-based materials, continued research is essential in developing greener synthesis techniques, effective catalyst management, and comprehensive lifecycle assessments. Although limited study has been performed on the interaction of carbon-based material such as graphene with the environment, it has been suggested that they can be biodegradable [33], therefore, offering the possibility of end-of-life disposal without the need for complex separation and recycling processes, especially when used in composites with other biodegradable polymers such as cellulose-based materials and polylactic acids.

While existing literature has reviewed carbon-based sensors, these reviews have typically focused on single-sensor functionalities (e.g., humidity, temperature, or mechanical sensors) and broadly addressed diverse applications ranging from environmental monitoring to healthcare wearables [34–40]. Existing reviews lack detailed discussions on novel carbon-based composite materials and advanced fabrication techniques developed specifically for packaging in relation to transportation conditions or transit. Equality, to the best of our knowledge, no previous review has simultaneously examined multiple sensing functionalities tailored to smart packaging for food and medical/pharmaceutical products. Furthermore, recent regulatory changes [41–43] coupled with technological advancements, alongside the growth of online shopping, have heightened the demand for specialized reviews on these applications to ensure compliance and efficacy. Consequently, there is a clear gap in the literature and this review significantly contributes to filling that by providing the first comprehensive and systematic analysis of recent advancements (2013–2024) in carbon-based humidity, temperature, mechanical, and multifunctional sensors for smart packaging applications for food and medical/pharmaceutical products that meet the acceptable conditions for safe storage and transportation (Table 1). Our review uniquely highlights the innovations in composite material design, structural optimization, and fabrication techniques that could enhance sensor performance specifically in packaging scenarios, offering new insights that bridge laboratory innovation with practical industrial scalability and regulatory compliance. Finally, the review identifies current research gaps and outlines potential future directions for cost-effective, scalable, and environmentally friendly on-package carbon-based sensors development in the food and pharmaceutical sectors.

2. Materials and Methods

The methodology for this review follows the guidelines of the Preferred Reporting Items for Systematic Reviews and Meta-Analyses (PRISMA) and the Prisma Checklist can be found in Supplementary Materials, Table S1. This offers a comprehensive review to ensure a comprehensive and focused analysis of recent advancements in carbon-based sensors [44]. It was registered in the Open Science Framework (https://doi.org/10.17605/OSF.IO/DYX4H, accessed on 2 April 2025).

2.1. Database Selection and Search Strategy

A comprehensive search was conducted across major academic databases, including Scopus, Web of Science, IEEE Xplore, and Wiley to ensure a broad coverage of relevant studies. The search strings were used to capture articles in all databases using a structured combination of keywords such as TITLE-ABS-KEY ('carbon-based' OR 'graphene-based' OR 'graphene' OR 'carbon nanotube' OR 'graphene oxide' OR 'CNT' OR 'carbon') AND TITLE-ABS-KEY ('temperature sensor' OR 'humidity sensor' OR 'mechanical sensor') AND TITLE-ABS-KEY (packaging AND food OR medical) AND PUBYEAR > 2013 AND PUBYEAR < 2025 AND (LIMIT-TO (DOCTYPE, 'ar')) AND (LIMIT-TO (LANGUAGE, 'English')).

2.2. Screening

After initial searching, a multi-step screening process was conducted. Firstly, after removing duplicates, each study was screened by titles and abstracts to access their potential relevance based on predefined inclusion and exclusion criteria (Table 2).

Table 2. Inclusion and exclusion criteria for the screening iterations.

Inclusion Criteria	Exclusion Criteria
Focus on carbon-based humidity, temperature, mechanical, and multifunctional sensors for food and medical or pharmaceutical smart packaging	Review articles, conference proceedings, books, and inaccessible articles
Articles discussing sensor improvement with sufficient details on sensor design, fabrication methods, and performance metrics	Unrelated to sensor performance or improvements
English language	Purely theoretical articles
The properties suitable for transportation in Table 1.	Articles that present speculative, unvalidated, or incomplete results
Access to full text via the authors' institution	Publication before 2013

Articles that met the inclusion criteria underwent a detailed full-text review to ensure alignment with the research objectives. To ensure comprehensiveness, citation screening was employed during the full-text review. References within selected articles were assessed to identify additional relevant articles not captured in the database search. Newly identified articles were subjected to the same screening and inclusion criteria.

2.3. Data Extraction

Data extraction was conducted by S.G. using Microsoft Excel for data synthesis and presentation. For each study, the critical information like carbon-based material type, sensor design, fabrication methods, and performance metrics (e.g., sensitivity, response time, operating range, and durability) were recorded and compiled into tables. Owing to the heterogeneity of study designs, only a qualitative assessment was employed.

3. Results

A total of 953 articles were screened, and after excluding duplicates and studies that did not meet the eligibility criteria, 163 relevant articles were identified. The complete selection process is shown in Figure 2. The PRISMA flow diagram illustrates the systematic review process, detailing the number of articles included and excluded at each stage. Among the relevant articles, 72 deal with humidity sensors, 45 with temperature sensors, 23 with mechanical sensors (10 pressure sensors and 13 strain sensors), and 23 articles related to carbon-based multifunctional sensors. Articles included in this review are largely from Journals of Quartiles, Q1 and Q2.

Identification of studies via databases

Identification

Records identified from database searching
(n = 867):
Scopus (n = 384)
Web of Science (n = 399)
IEEE Xplore (n = 84)

→ Duplicate records removed
(n = 390)

Identification citation via selected eligible articles

Records identified from:
Citation searching
(n = 86)
Humidity sensor (n= 62)
Temperature sensor (n= 15)
Mechanical sensor (n= 5)
Multifunctional sensor (n= 4)

Screening

Records screened
(n = 477)
Humidity sensor (n= 166)
Temperature sensor (n= 131)
Mechanical sensor (n= 105)
Multifunctional sensor (n= 75)

→ Records excluded based on title/abstract screening
(n = 201)

Eligibility

Full-text articles assessed for eligibility
(n = 276)
Humidity (n= 90)
Temperature (n= 57)
Mechanical (n= 76)
Multifunctional (n= 53)

→ Full-text articles excluded due to scope and insufficient detail
(n= 132):
Humidity (n= 29)
Temperature (n= 17)
Mechanical (n= 58)
Multifunctional (n= 31)

Full-text articles assessed for eligibility
(n = 22)
Humidity (n= 11)
Temperature (n= 5)
Mechanical (n= 5)
Multifunctional (n= 1)

→ Full-text articles excluded due to scope and insufficient details
(n= 64)

Included

Studies included in review
(n = 163)
Humidity sensor (n= 72)
Temperature sensor (n= 45)
Mechanical sensor (n= 23)
Multifunctional sensor (n= 23)

Figure 2. Flow diagram of the adapted PRISMA approach used in this study capturing screening step and results.

3.1. Humidity Sensors

Table 3 summarizes 72 carbon-based humidity sensors with potential application in packaging for food and medical/pharmaceutical products, detailing the materials used, production methods, and resulting properties.

Among the carbon materials studied, GO-based sensors were the most commonly used (33 studies) [45–77], followed by graphene (17 studies) [78–94], rGO (8 studies) [95–103], CNTs (7 studies) [68,76,104–108] and GQDs (4 studies) [109–112]. Sensor performance is frequently enhanced by incorporating carbon-based materials with polymers, metal oxides, specific dopants, and advanced nanostructural materials. A shift is noted from metal- to carbon-based electrodes, such as graphene [67,84,85], GO [77], rGO [97], Laser induced

graphene (LIG) [53,54,62,78], carbon [113], CNTs [72], and their composites [77], to support cost reduction and improve flexibility and durability.

The fabrication techniques are diverse and tailored to different sensor configurations and specific performance. Key methods include drop-casting, spin-coating, and screen-printing created uniform films, whereas electrospinning, laser scribing, hydrothermal techniques form 3D or textured structures. The main types of investigated humidity sensors are resistive (29 studies), capacitive (18 studies), and impedance (11 studies), with a growing interest in hybrid configurations, which combine different sensing mechanisms for improved environmental adaptability.

Many carbon-based humidity sensors operate effectively across 10–97%RH, and some sensors like oxidized carbon nanohorns/graphene oxides/Tin Oxide/Poly(vinylpyrrolidone) (CNH/GO/SnO$_2$/PVP) [47], GO/oxidized CNH/PVP [48], and molybdenum ditelluride/graphene (MoS$_2$/graphene) [78], extended to 0–100%RH detection. In contrast, several sensors, such as N-S co-doped GQDs, have a narrow range (40–90%RH) with optimized performance [110]. Sensitivity varies significantly based on material composition and structure, ranging from 0.022 for ZnO/PVP-rGO [96] to 9,750,000% for paper cellulose fiber/GO [77].

The response and recovery time is essential for real-time monitoring and the values vary from 0.02 s for nanocrystalline graphite [114] to 333 s for TEMPO-oxidized cellulose fibers/carbon nanotubes (TOCFs/CNTs) [106]. Capacitive sensors generally show faster response times than resistive and impedance sensors. Notably, 18 sensors, including ZnO/PVP-rGO nanocomposite demonstrated faster recovery than response time [53–55,57–59,63,64,70–72,75,77,78,82,96,101,111].

The selectivity of carbon-based sensors is key in ensuring reliable sensor performance under real-world conditions. The reviewed studies [46,52,55,59,62,88,113] demonstrated high selectivity to water vapor through material modifications such as doping, composite integration, and surface functionalization. The reusability, inferred from stable performance under repeated humidity cycles, is indirectly supported by the stability and durability data, though direct cyclic reuse metrics have not been reported.

Sensor stability is crucial for consistent sensor performance in different transportation scenarios of products whereas low hysteresis is important for its long-term reliability. The stability was up to 1095 days for laser-reduced GO/MWCNT sensors, fabricated using a 785 nm, 5 mW laser with a 50 μm spot size under Direct Laser-Scribed (DLS) conditions [97]. The reliability remains around 3–8% for most sensors, with the exception of Li-doped GO achieving 0.83% [45]. Some sensors, such those with GO functionalized with hydroxyl groups [46], shellac-derived carbon thin film [113], oxidized CNH/GO/SnO$_2$/PVP nanocomposite [47], and GO-oxidized CNH-PVP [48] consuming 15 μW [46] to 2 mW, could be ideal for prolonged monitoring. This is a very useful feature as low power consumption sensors are advantageous in many respects from a sustainability and environmental standpoint as well as for system miniaturization.

Table 3. Summary of different humidity sensors reported in the literature with their resulting properties including the sensing range, sensitivity, durability, linearity, response, and recovery time.

Material	Fabrication Technique	Type	Sensing Range (%RH)	Sensitivity	Response/Recovery Time (s)	Stability (Days)	Linearity	Remarks/Comments	Ref
Li-doped GO			11–97	17.13–3038.16%	4/25	Not reported (N)	Yes	Hysteresis is 0.83% and thermal stability is 850 °C.	[45]
GO functionalized with hydroxyl groups		Resistive	6–95	~38.5	8.5/13	390	Yes	Hysteresis is 0.63%. High selectivity to humidity. Power consumption is 15 μW.	[46]
Oxidized CNH/GO/SnO$_2$/PVP nanocomposite film	Drop casting		0–100	0.9021 Ω/% RH	42/164	N	Yes	CNHox/GO/SnO$_2$/PVP mass ratio is 1/1/1/1. Power consumption is <2 mW.	[47]
GO-oxidized CNH-PVP			0–100	0.15–0.2	40–90/62–73	N	Yes	Optimal GO:CNH:PVP is 1:1:1. Power consumption is <2 mW.	[48]
Ultra-thin, single-layer GO film			10%–95	120.57%/%RH	0.49/0.65	60	No	Optimal sensor has 300 nm GO with 20 μm electrodes spacing.	[49]
Oxidized single-walled carbon nanohorns (SWCNHs)			10–90	~2.1×10^7 Ω/RH (air) ~9.1×10^6 Ω/RH (N$_2$)	3/N (air) 8/N (N$_2$)	N	Yes	Surface area is 1300–1400 m^2/g.	[115]
GO/PVA composite		Resistive Frequency	20–80	−12,000 Ω/%RH 0.0001 kHz/%RH	N	N	N	It achieves ~1.8% RH resolution.	[50]
rGO/PVDF composite	Solution casting	Resistive	11–97	98.99%	21/26	90	Yes	Optimal is 30 vol% rGO/PVDF. Hysteresis is 5.5% and decomposition from 434° C.	[95]
Endohedral lithium-doped SWCNT/sodium dodecylbenzenesulfonate (Li@SWCNT/SDBS)	Arc discharge and drop casting		11–97	4%/%RH	N	N	No	Optimal sensor is five-layer thin film (~5 μm thickness). Hysteresis is 4.3%.	[104]
GQDs/Ag nanoparticles (AgNPs)	Hydrothermal and drop casting		25–95	98.14%	15/15	N	No	Optimal GQDs/AgNPs is 1:1.	[109]

Table 3. *Cont.*

Material	Fabrication Technique	Type	Sensing Range (%RH)	Sensitivity	Response/ Recovery Time (s)	Stability (Days)	Linearity	Remarks/Comments	Ref
GO film			15–95	37,800%	10.5/41	30	Yes	Hysteresis is ~5%.	[51]
GO/Ag composite		Capacitive	11–97	25,809 pF/%RH	~8/~12	30	N	Optimal Ag content is 2 wt%. Good selectivity for H_2O vapor.	[52]
GO			0–97	1800 pF/% RH	16/9	N	Yes	Spiral LIG as electrodes. Optimal GO thickness is 50 nm. 3.03% hysteresis.	[53]
GO	Drop casting		10–90	3862 pF/%RH	58/15	42	N	Hysteresis is 1.2%. Optimal sensor used 60 μL GO and 150 μm gap size for LIG interdigitated electrodes (IDE).	[54]
GO/MoTe$_2$ composite nanosheets			11.3–97.3	94.12 pF/%RH	39/12	35	N	Optimal GO to MoTe$_2$ ratio is 1:2. High humidity selectivity.	[55]
ZnO/PVP-rGO nanocomposite		Capacitive	15–95	~0.022	~12/~3	87	Yes		[96]
GO-Mn-doped ZnO nanocomposite		Capacitive Resistive	10–90	N	4.5/21	30	Yes	95.7 times higher sensitivity in capacitance and 97 times in resistance compared to conventional GO.	[56]
GO-doped P(VDF-TrFE)/LiCl composite		Capacitive change	25–95	1708.8 pF/%RH	7.8/4.5	N	Yes	Pores from 300 nm to 1.1 μm. Reduced hysteresis due to GO and LiCl modification.	[57]
GO		Resonant frequency	10–90	0.719 kHz/%RH	<78/54	30	No	Resolution (0.4% RH), hysteresis (<4%), and minimal response to CO_2.	[58]
HGO/GO/Mg^{2+} composite membrane			11–97	0.0343 kHz/%RH	7/6	10	Yes	Hysteresis is ~3.2% RH. High humidity selectivity.	[59]
GO		Voltage	33–98	1.1–10.0 mV/%RH	0.28/0.3	2.5	Yes	GO thickness is 10 μm.	[61]
2D MoS$_2$/graphene nanocomposite foam		Impedance	0–100	50,000– 385,000 Ω/%RH	4/2	N	No	Sensor used LIG as electrodes. Hysteresis is 3.8%.	[78]
Laser-reduced GO/MWCNT	Drop casting and direct laser scribing	Impedance Capacitance	11–97	350,000 Ω/%RH 798 pF/%RHc	0.061/2.3	1095	Yes	Sensor used rGO IDE. Hysteresis is 3.1%.	[97]

Table 3. *Cont.*

Material	Fabrication Technique	Type	Sensing Range (%RH)	Sensitivity	Response/Recovery Time (s)	Stability (Days)	Linearity	Remarks/Comments	Ref
Thermally reduced GO	Spin-coating	Resistive	32–65	5%	35/N	N	Yes	Highly thermal-reduced GO has the optimal performance.	[98]
P(VDF-TrFE) with graphene flower composite	Spin-coating	Capacitance Impedance	8–98	0.0558 pF/% RH	0.8/2.5	15	Yes	N	[79]
GO		Impedance	6–97	182,068.791/%RH	0.8/0.9	1	Yes	$Ti_3C_2T_x$ MXene-based sensor exhibited faster response than sensors using metallic electrodes.	[60]
N-S co-doped GQDs	Hydrothermal and spin-coating		40–90	N	15/55	90	N	Optimal GQDs content is 10 mg with 2.2% hysteresis.	[110]
GQDs/carbon nitride (g-C3N4) composite			7–97	100,000 Ω/RH	44 /10	N	Yes	Low hysteresis (<1%) and high surface area (545 m^2/g)	[111]
Bi-layered PVA/graphene flower composite film	Spin-coating and spray-coating	Capacitance Impedance	40–90	29,000 pF/%RH	2/3.5	15	N	Uniform dispersion of PVA/GF layer with ~2.32 μm thickness.	[80]
Shellac-derived carbon (SDC) thin film	Spray coating and thermal annealing	Resistive	0–90	0.54/% RH	0.14/1.7	28	Yes	Carbon IDE. High selective to humidity. Power consumption is ~1 mW.	[113]
rGO-sodium dodecyl sulfate (SDS) composite film	Drop-coating	Resistive	25–95	11.4143 Ω/% RH (RT)	9/10	10	Yes	Hysteresis is 0.04852%.	[99]
GO			11–97	1.113 Ω/Ω–%RH	2/35	N	Yes	Sensor used 300 nm wrinkled GO film on the LIG electrode. Hysteresis is 3%. High humidity selectivity.	[62]
GO		Quartz crystal microbalance (QCM)	11.3–97.3	0.1605 kHz/%RH	30/5	N	Yes	The study used the finite element analysis software COMSOL Multiphysics.	[63]
Polydopamine-coated cellulose nanocrystals/GO nanocomposite (PDA@CNC/GO)	Drop-coating	Resonance frequency	11.3–97.3	0.05466 kHz/% RH	37/5	21	N	Optimal composition is 30 wt% PDA@CNC. Hysteresis is 4.3% RH.	[64]

Table 3. *Cont.*

Material	Fabrication Technique	Type	Sensing Range (%RH)	Sensitivity	Response/ Recovery Time (s)	Stability (Days)	Linearity	Remarks/Comments	Ref
Graphene flower/ZnO composite	Sol–gel and spray-coating	Resistive	15–86	7.7 μA/%RH	0.4/4	N	N	High surface area to volume ratio and pore composite.	[81]
GO on tilted fiber grating (TFG)	Dip-coating	Resonance wavelength Intensity	30–80	0.0185 nm/%RH	0.042/0.115	N	Yes	GO thickness is 54 nm.	[65]
GO/PVA composite film		Intensity	20–99.9	0.529 RH (%)	147/293	N	Yes	N	[66]
Graphene–carbon ink	Screen printing	Resistive	25–91.7	12.4 Ω/%RH	~31/~8	120	N	Optimal configuration is single-layer sensor.	[82]
G/polypyrrole/carbon black (CB) composite			23–92.7	12.2 Ω/%RH	5/7	21	N	Durability is 100 bending cycles Single-layer is the most effective configuration.	[83]
Graphite/WO$_3$ nanocomposite			11–97	12.7–60.8%	N	N	Yes	Optimal sensor using graphite/WO$_3$ ratio is 1:3, with <1% hysteresis. 120° bending angles.	[116]
Multilayer GO		Resonance frequency Backscattered phase	11–98	0.5°/%RH	N	N	N	30 μm GO film and printed graphene antenna electrodes.	[67]
Cellulose nanofiber (CNF) and graphene nanoplatelet (GNP) composite	Mixing and screen printing	Resistive	30–90	240%	17/22	240	N	Composite with 200 mg GNP as electrode.	[84]
Graphene ink	Inkjet printing	Capacitive	10–70	0.03 pF/%RH	2.46/2.63	10	N	Optimal sensor is six-layer graphene film with graphene IDEs.	[85]
GO/CNT−OH/Nafion nanocomposite		Resonance frequency	30–95	547 kHz/%RH	110/115	2.08	Yes	Hysteresis is 3%.	[68]
Functionalized MWCNTs and hydroxyethyl cellulose (HEC) composite	Gravure printing	Resistive	20–80	0.0485/%RH	20/35	0.4	Yes	The optimal FMWCNT concentration is 2.5 wt%.	[105]

Table 3. *Cont.*

Material	Fabrication Technique	Type	Sensing Range (%RH)	Sensitivity	Response/Recovery Time (s)	Stability (Days)	Linearity	Remarks/Comments	Ref
Carboxymethyl cellulose@graphene (CMC/G) composite	3D printed groove mold	Impedance	11–95	97%	300/N	16	Yes	Optimal graphene content is 0.16 wt%.	[86]
Graphene film	Liquid phase exfoliation and LB assembly	Resistive	8–95	5%	0.028/0.03	N	Yes	The thickness is ~3.4 nm (~ 10 layers). Flexibility is 10° bending.	[87]
GO	Self-assembly	Capacitive	30–90	0.00565 pF/% RH	180/N	14	N	Optimal sensor is 2 mg/mL GO with 2.85% hysteresis.	[69]
Pyranine modified-rGO composite	One-step supramolecular assembly	Impedance	11–95	IL/IH = 6000	<2/~6	N	Yes	Hysteresis is 8% RH. Stable for 100 cycles.	[100]
TEMPO-oxidized cellulose fibers (TOCFs)/CNTs	Electrostatic self-assembly	Current	11–95	87%	333/523	90	Yes	Optimal TOCFs-to-CNTs ratio is 30:1 with a thickness of 48.2 μm and 7.3% hysteresis.	[106]
G with 3D flower-like ZnO composite	Hydrothermal	Impedance	12–90	446	120/160	30	N	Optimal G content is 70 wt% with 2.32% hysteresis. High humidity selectivity.	[88]
PVDF (polyvinylidene fluoride) with 0.5 wt% G	Electrospinning	Capacitive	35–90	0.0463 pF/%RH	N	N	Yes	PVDF/G with Ag electrode, showed 21.3 times faster than DHT11.	[89]
SnO$_2$/rGO nanocomposite			11–95	37,491%	80/4	N	N	Optimal rGO doping content is 2 wt%. Durability is 1000 bending cycles.	[101]
BP/G hybrid	Electrospray	Resistive	15–70	43.40%	9/30	28	Yes		[90]
GO	Electrospray deposition	Resonant frequency	11–97	1.74%/%RH	54–68/12–22	30	No	Low thermal noise. Optimal is 250 MHz sensor.	[70]
Holey-reduced graphene oxide (HRGO)	H$_2$O$_2$-etching-reaction-assisted hydrothermal	Impedance	11–97	−0.04317 log Z/%RH	<3/29	28	Yes	Surface area is 274.5 m^2/g. Hysteresis is 2.57%.	[102]
GO	Dripping and vacuum heating	Capacitive	20–90	1.77–164.98 pF/% RH	10/2	N	N	Hysteresis is 1%.	[71]

Table 3. *Cont.*

Material	Fabrication Technique	Type	Sensing Range (%RH)	Sensitivity	Response/Recovery Time (s)	Stability (Days)	Linearity	Remarks/Comments	Ref
GO	Dripping and coating		10–90	16.7 pF/%RH	0.0208/0.0199	80	N	The optimal sensor used 1 mg/mL GO and CNTs as electrodes. Hysteresis (<0.44%).	[72]
ZnO nanowires and GQDs composite	Dripping	Resonance frequency	30–90	40.16 kHz/%RH	~30/~35	N	No	Optimal GQDs content is 2 mg/mL. 30° bending angle.	[112]
SWCNTs	Vacuum filtration	Resistive	15–98	246.90%	290/510	N	Yes	Optimal sensor is suspended aligned. SWCNT beams, with 36 μm suspension lengths.	[107]
rGO/PANI composite	Filtration		0–98	580%	~70/~139	N	Yes	Hysteresis is 3%. Optimal rGO to PANI ratio is 5%.	[103]
Laser-induced graphene (LIG)	Laser Direct Writing (LDW)	Capacitive	30–90	N	8/10	N	No	The porous, hair-like LIG pattern was designed with 2-CAD.	[91]
Light-scribed GO	Laser scribe	Impedance	7–97	1.67×10^6 Ω/%RH	N	1	Yes	Hysteresis is 0.3–7%.	[73]
G/ZrO$_2$ nanocomposite	Sol–gel		12–90	4011	5/20	6	Yes	Hysteresis is <1.95%. Optimal is 40 wt% G/ZrO$_2$	[92]
3D graphene foam	Modified Hummers' method	Resistive	0–85.9	N	0.089/0.189	N	N	Energy structure of 3DGF model analyzed via CASTEP in Materials Studio 8.0.	[93]
Nanocrystalline graphite	Plasma-enhanced CVD		15–85	0.0334%/%RH	0.02/N	N	Yes	Hysteresis is 5%. It is meandered strip structure.	[114]
SWCNT	Immersion	Resistive	20–80	54.7% (s-CNT) 2.9% (m-CNT)	40/100	N	Yes	Hysteresis is 11.45% (semiconducting-CNT) and 0.31% (metallic-CNT).	[108]
G/p-aminophenol/poly-2-hydroxyethyl acrylate (G/p-AP/PHEA)	In situ free-radical polymerization		0–94	29%	N	N	N	N	[94]
Etched GO film	Etching	Capacitive	10–100	0.000106 pF/% RH	1.011/N	N	N	The study using COMSOL Multiphysics.	[74]

Table 3. *Cont.*

Material	Fabrication Technique	Type	Sensing Range (%RH)	Sensitivity	Response/ Recovery Time (s)	Stability (Days)	Linearity	Remarks/Comments	Ref
Nanofibrillated cellulose (NFC)/GO/PDMS aerogel composite	Ultrasonic dispersion and freeze-drying		11–97	6576.41 pF/% RH	57/2	N	No	Porosity is 99.6%.	[75]
GO/MWCNTs hybrid on tilted Fiber Bragg Grating (TFBG)	Physical precipitation	Optical fiber Amplitude	30–90	0.377 dB/%RH	4/N	N	Yes	Hysteresis is 0.7%.	[76]
Paper cellulose fiber/GO matrix (PCFGOM)	N	Impedance Capacitance	10–90	9,750,000% (1 kHz) 1,442,500% (10 kHz)	1.3 /0.8	1	Yes	The sensor used 0.15 w/w% PCFGOM as active layer and 20 w/w% PCFGOM as electrode layers.	[77]

3.2. Temperature Sensors

Table 4 summarizes 45 carbon-based temperature sensors with their composition, production methods, and resulting properties. Graphene-based sensors were predominant among the reported studied (19 studies) [117–135], followed by rGO (11 studies) [123,136–145], CNTs (9 studies) [146–154], and GO (4 studies) [155–158]. Other carbon materials, including GQDs [159], carbon dots (CDs) [160], and amorphous carbon [161] were reported in only one study, respectively, highlighting their limited exploration in this field. The incorporation of polymers and metals/metal oxides into carbon-based materials has been extensively explored to enhance the performance of temperature sensors. The combination with metal/metal oxides were predominantly applied to rGO [138,141,145] and graphene [128]. In contrast, polymers like Poly(3,4-ethylenedioxythiophene) polystyrene sulfonate (PEDOT:PSS), polydimethylsiloxane (PDMS), and gelatine were widely combined with various carbon materials, including graphene (6 studies) [118–122,135], GO (2 studies) [157,158], rGO (3 studies) [140,143,144], and CNTs (5 studies) [146–148,150,151].

Chemical vapor deposition (CVD) was the most dominant method (10 studies) [123, 127–132,151–153], particularly for graphene and CNT sensors. Methods of coating (12 studies) [117–124,136,137,146,155] including spray coating [117,123,124,136], drop casting (5 studies) [138,147,148,155,156], and printing (6 studies) [139–141,149,150,157] was widely used in rGO, GO, and composite sensors, offering simplicity and scalability.

Graphene-based sensors fabricated via CVD exhibited the broadest detection ranges, spanning from -266.55 °C [129] to 302 °C [130], quick response time of ~0.030 s in multilayer graphene [129], and high sensitivities, such as 2.15 Ω/°C in micro-fabricated single-layer graphene [127]. Similarly, rGO-based sensors demonstrated wide detection range of -196.15–299.85 °C in rGO sensor [137], with exceptional sensitivity values of up to 1999%/°C for GQDs/rGO/alumina composite [142]. In contrast, GO-based sensors [155–158] and CNT-based sensors [146–148,150–153] generally operate within narrower ranges, typically starting at 20 °C, limiting their suitability for applications in chill- and cold-chain environments. However, functionalization and advanced fabrication methods have shown potential in improving detection capabilities. For instance, carboxyl-SWCNTs achieved a range of 0–80 °C but showed slow response (176.4 s) and recovery time (316.8 s) [154] whereas CNTs produced using gravure printing demonstrated a broader temperature range (-40–100 °C) and fast response (0.3 s) and recovery time (4 s) [149].

Response times varied significantly from 0.030 s for multilayer graphene produced by CVD [129] to 306 s for uncovered drop-casted GO sensors [155] depending on the material and encapsulation approach. Composite systems often outperformed pure carbon materials in detection range, sensitives, and responsiveness, particularly those combined with metal or metal oxides. For example, rGO/Ag exhibited extended temperature sensing ranges (-60–80 °C), faster response times (0.47 s), and good sensitivity (0.555 Ω/°C) [138].

Long-term stability was assessed in 10 studies [121,126,138,140,143,146,147,152,156,158], rGO/Ag nanocomposite with Parylene encapsulation demonstrating exceptional longevity, maintaining performance over 730 days durability [138].

Table 4. Summary of different temperature sensors reported in the literature with their resulting properties including sensing range, sensitivity, stability, response, and recovery time.

Material	Fabrication Technique	Sensing Range (°C)	Sensitivity/TCR (%/°C)	Response/ Recovery Time (s)	Stability (Days)	Remarks/Comments	Ref
GO	Drop casting	20–70	822 Ω/°C	306/554 (uncovered)	N	Encapsulation: PDMS	[155]
	Spray coating	20–60	N	0.525/0.35 (uncovered) 5.18/9.68 (covered)			
rGO	Spray coating	30–100	0.6345%/°C	1.2/N	N	Encapsulation: high-temperature transparent insulating tape.	[136]
Multilayer graphene ink film		30–90	43.27 μV/K	0.15 /15	N	Optimal sensors have 108 nm thickness and provide 300 μV output voltage, and signal-to-noise ratio is 35.	[117]
rGO	Spin coating	−196.15–299.85	−0.801−−32.04%/°C	52/285	N	Optimal rGO concentration is 3wt%, with 0.1 °C resolution.	[137]
MWCNT doped in polyethylene glycol and PU (MWCNT-PEG-PU) nanocomposites		25–50	~80%	N	7	Optimal MWCNT concentration is 8 wt% and stable 30 bending cycles.	[146]
Graphene-coated microfiber (GCM)	Coating	22–40	2.1 dB/°C	N	N	Minimum resolution is 0.0005 °C.	[118]
Polyaniline/graphene (GPANI) embedded in Polyvinyl Butyral (PVB) composite film	Coating using Mayer rod	25–80 °C	−1.2%/°C	N	N	Sensor also responds to external pressures (0–30 kPa). Encapsulation: Bezel tape	[119]

Table 4. *Cont.*

Material	Fabrication Technique	Sensing Range (°C)	Sensitivity/TCR (%/°C)	Response/ Recovery Time (s)	Stability (Days)	Remarks/Comments	Ref
Graphene and gelatin nanocomposite	Blade coating	−13–37	−5.3–−23 mV/°C	10.4/N	N	Stable for 20 cycles.	[120]
Graphene/gelatin nanocomposite		−13–37	−19 mV/K	41.8/N (pristine sensor)	2	Energy consumption is 8.1 μWh for pristine sensor.	[121]
				28.9/N (aged sensor)		Energy consumption is 8.5 μWh for aged devices.	
PU/G Nanocomposite	In situ polymerization and dip coating	25–60	6 pm/°C	N	N	Thermal stability to 217 °C from 204 °C.	[122]
rGO	Air brush spray coating		45.1%	121/N			
Graphene nanoplatelets (GNP)		0–100	52%	89/N	N	N	[123]
Plasma-grown graphene (Gpl)	Plasma discharge		20.5%	125/N			
Graphene via CVD (Gcvd)	CVD		27%	68/N			
GO	Post-COMS MEMS Drop casting	−70–40	155.73–58,555.26 pF/°C	Not reported (N)	30	Capacitance sensor.	[156]
rGO/Ag nanocomposite	Ultrasonication and drop casting	−60–80	0.555 Ω/°C	0.47/N (cold) 3.45/N (hot)	730	Encapsulation: Parylene.	[138]
CNT/PEDOT:PSS composite	Drop casting	25–45	−1.97%/°C (initial) −2.80%/°C (6 days aging)	N	6	Encapsulation: PDMS Optimal CNT/PEDOT ratios is 1:5.	[147]
CNT and methylcellulose (CNT/MC) composite	Solution casting	20–70	0.2%/°C	6.1/3.1 (hot) 5.2/7.2 (ice)	N	Stable over 480 cycles.	[148]
Graphene Nanoribbons (GNRs)	Mask spraying or direct handwriting	30–80	172% TCR = 1.27%/°C	0.5/0.5	N	Using MWCNT ink electrodes and Scotch tape encapsulation. 0.2 °C resolution and stable 5000 bending cycles.	[124]
CNT	Gravure printing	−40–100	−0.4%/°C	0.3/4	N	High accuracy (±0.5 °C). Encapsulation: organic and silver.	[149]

Table 4. *Cont.*

Material	Fabrication Technique	Sensing Range (°C)	Sensitivity/TCR (%/°C)	Response/ Recovery Time (s)	Stability (Days)	Remarks/Comments	Ref
GO/PEDOT: PSS composite	Mask printing	25–100	−1.09%/°C	18/32	N	Encapsulation: Kapton tape. Stable 1000 bending cycles.	[157]
Functionalized and reduced graphene oxide via sulfonated aromatic diamine (f-rGO)	Inkjet printing	30–82	−0.0164/°C	176.4/316.8	N		[139]
CNT/PEDOT-PSS composite		25–50	0.31%/°C	~39/~196	N	Encapsulation: translucent polyurethane welding tape. Stable 1000 cycles bending.	[150]
rGO with alkali lignin		25–135	0.59%/°C	N	180	Sensor used meander-shaped rGO as electrode.	[140]
rGO/Ag	Aerosol jet printing	0–200	0.001162–0.001519/°C	N	N	Optimal four layers rGO/Ag. Stable 1000 bending cycles.	[141]
Porous LIG	CO_2 laser-induced Direct laser writing	1–8	N	16/58	N	Encapsulation: PDMS. Stable 200 bending cycles.	[125]
LIG	Laser direct writing	24–80	−0.58%/°C	N	14	Sensors optimized by finite element analysis photothermal model.	[126]
Amorphous carbon films	DC Magnetron Sputtering	20–150	1.62 mV/°C TCR = 0.00128/°C	N	N	DC magnetron sputtered sensors are more stable and practical than ion-beam-deposited sensor.	[161]
Micro-fabricated single-layer graphene	CVD	10–30	1.25 Ω/°C (SiO_2/Si substrate) 2.15 Ω/°C (SiN substrate) 1.90 Ω/°C (suspended graphene substrate)	N	N	Sensor used graphene electrodes and PDMS gasket encapsulation.	[127]
CNT forest-PDMS composite		30–90	0.55 Ω/°C	N	N	Encapsulation: PDMS.	[151]
Graphene and Lithium Niobate ($LiNbO_3$)		10–70	−0.23 nm/°C	N	N	Encapsulation: PDMS.	[128]

Table 4. *Cont.*

Material	Fabrication Technique	Sensing Range (°C)	Sensitivity/TCR (%/°C)	Response/ Recovery Time (s)	Stability (Days)	Remarks/Comments	Ref
Multilayer graphene		−266.55–26.85	−1 (THS < −243.15 °C) <0.1 (THS > −173.15 °C)	~0.030/N	N	Sensor made by seven layers of single-layer graphene.	[129]
Vertically aligned CNT film	TCVD	20–110	4.74 μA/°C (air) 22.72 μA/°C (N_2)	N	30	Triple-electrode structure enables long-term sensor operation.	[152]
MWCNT		22–200	0.0033 V/°C TCR = 0.00103/°C	N	N	2.7 μm MWCNT sensor had carrier mobility (−28.5574 cm^2/Vs).	[153]
Single-layer graphene	CVD and wet transfer	27–302	0.00207/°C (27–177 °C) 0.00239/°C (177–302 °C)	N	N	Resistance is almost unaffected by humidity.	[130]
Suspended few-layer and multilayer graphene		25–120	1.07–3.5%/°C	N	N	N	[131]
Graphene	CVD and AI sacrificial layer process	25–200	2.134 Ω/°C	N	N	Enhanced 41.93% consistency. Encapsulation: SiO_2 layer.	[132]
GQDs embedded in a rGO/alumina composite film	Sol–gel	−196.15–26.85 26.85–99.85	−1999%/°C −0.98%/°C	~0.3/0.8 3.96/6.01	N	Short-term stability is 50 cycles.	[142]
CNC-assisted carbon dots (CDs)-grafted $SrAl_2O_4$: Eu^{2+}, Dy^{3+} (SAO) phosphors composite film	Sol–gel and vacuum filtration	−30–110	0.257	N	N	Short-term stability is 3.5 cycles.	[160]
High-strength metallurgical graphene (HSMG)	Modified PMMA-based transfer	−253.15–21.85	−0.007/°C	N	N	Encapsulation: transparent polymer.	[133]
Polyethyleneimine/reduced graphene oxide (PEI/rGO)	Spray dipping	25–45 0–60	1.3%/°C	0.33–0.443/N	120	Encapsulation: PDMS. 0.1 °C resolution and 500 bending cycle stability.	[143]
GO/PEDOT: PSS micro/nanowires	Soft lithography	30–80	−0.007599/°C	3.5 /13.4	30	Optimal GO doping ratio is 13:1.	[158]
LIG	CO_2 laser irradiation	30–60	−0.04145%/°C	30/N	N	High measurement accuracy (±0.15 °C).	[134]

Table 4. *Cont.*

Material	Fabrication Technique	Sensing Range (°C)	Sensitivity/TCR (%/°C)	Response/ Recovery Time (s)	Stability (Days)	Remarks/Comments	Ref
PDA-rGO/sodium alginate/polyacrylamide composite organohydrogel	Solvent displacement and cross-linking	−20–60	97.6%/°C (−20–−5 °C) 10.57%/°C (−5–15 °C) 1.45%/°C (15–60 °C)	0.2/0.3	N	Encapsulation: VHB tape. Stable over 3 h.	[144]
Star-like rGO/SnO$_2$/Co$_3$O$_4$ composite	Facile wet chemical precipitation	25–125	0.561%/°C	N	N		[145]
GNP/PDMS nanocomposite	Three-roll milling and molding	30–80	0.052–11.7/°C	N	N	The optimal GNP concentration is 6 wt%.	[135]
Carboxyl-SWCNTs	N	0–80	−225 Ω/°C	N	N	Encapsulation: thermos-reversible polymer. Self-healing 30 bending cycles.	[154]
GQDs/hollow-core fiber	N	10–80	−0.01375/°C	N	N	N	[159]

3.3. Mechanical Sensors

The review revealed 10 carbon-based pressure sensors that could be used to monitor internal and external forces exerted on packaging as well as 13 carbon-based strain sensors. These findings are summarized in Tables 5 and 6, respectively.

Similarly to temperature sensors, graphene-based sensors dominate the literature (4 studies) [162–165] while other carbon materials, including GO [166], rGO [167], CNTs [168], carbon-ink [169], and CB [170] were reported in only one study each. A total of 70% of sensors were porous composite materials that mainly harness the high conductivity and mechanical strength of carbon materials alongside the flexibility, stretchability, and durability of polymers. However, some pressure sensors were produced with only graphene films via CVD [162,163]. The sensor production methods range from simple techniques such as molding [164,167,171], dip coating [169], self-assembly [166], and solvent extraction [165] to relatively more advanced fabrication techniques such as laser thermoforming [170], electrospinning and mechanical drawing [168].

The sensing range depends on materials and structure design, spanning from 20 kPa [167] to 20,000 kPa in a graphene N/MEMS mechanical sensor with crossbeam structure [163]. Porous structures such as porous PDMS [171], graphene/PDMS sponge [164], and polyurethane/graphene (PU/G) foams [165] reach up to 500 kPa, while softer materials such as tannic acid-reduced graphene oxide combined with polyvinyl alcohol (TArGO/PVA) hydrogel [167] and nitrogen-doped graphene oxide/dopamine/polyaniline (GO/DA/PANI) aerogel [166] are limited to 20–25.48 kPa, which restricts their use to low-pressure environments and modified atmosphere packaging. Film structures like monolayer graphene have narrow sensing range, up to 80 kPa [162].

The sensor sensitivity also varies, with the formulation and production conditions ranging from 0.0259 kPa^{-1} [169] to 2200 kHz/kPa [164]. High sensitivity was observed at low pressures and this decreased as the pressure increased, particularly in composites with wide detecting range. Indeed, the sensitivity of a graphene/PDMS composite decreases from 2200 kHz/kPa at 0–10 kPa to 37.5 kHz/kPa at 200–500 kPa [164]. The incorporation of carbon black and use of glucose monohydrate to form porous PDMS/graphene composite contributed to improved flexibility and sensitivity (109.4 kPa^{-1}) of the sensor [170]. Fluoropolymers such as Poly (vinylidene fluoride) (PVDF) and its copolymer poly(vinylidene fluoride-trifluoroethylene) (P(VDF-TrFE)) with SWCNTs or MWCNTs have also been used with reasonable sensitivity. However, recycling or reusing PVDF components when they reach the end of their useful lives is particularly challenging, whereas their disposal by incineration poses an environmental issue because of the potential formation of hydrogen fluoride at elevated temperatures [172].

The durability varies from 100 cycles for hydrogels [167] to 10,000 cycles for porous composites like PDMS/graphene [171]. Response and recovery times varied across materials and sensor structures, and graphene/PDMS sponge achieved fastest response time of 7 ms with 60 ms recovery time [164], while porous PDMS with MWCNT/PEDOT electrode showed 1 s of response and recovery time [171].

Table 5. Summary of different pressure sensors reported in the literature with their fabrication methods and resulting properties including the sensing range, sensitivity, durability, response and recovery time.

Material	Fabrication Technique	Sensing Range (kPa)	Sensitivity/Gauge Factor (GF)	Response/ Recovery Time (s)	Durability (Cycles)	Remarks/Comments	Ref
Suspended monolayer graphene (G)	CVD	0–80	GF = 6.73 (circular membrane) GF = 3.91 (rectangular membrane)	Not reported (N)	Not reported (N)	An improved theoretical model was developed to predict GF and confirm their independence of doping concentration and graphene crystallographic orientation.	[162]
Graphene	Plasma-enhanced CVD	0–20,000	0.03313 mV/V/kPa GF = ~1.35	N	35 days	Encapsulation: Si_3N_4 film. Error of hysteresis (2.0119%), nonlinear (3.3622%), and repeatability (4.0271%).	[163]
Graphene/PDMS sponge	Mixing and molding	0.005–500	37.5–2200 kHz/kPa	~0.007/0.06	5000	LC technology used for long-distance wireless transmission. Optimal graphene concentration is 20%.	[164]
Porous PDMS	Sugar-cube mold	0–1200	360–1120 kPa^{-1}	1/<1	10,000	Sensor used MWCNT/PEDOT composite electrode and low-pass filter.	[171]
Tannic acid (TA)-rGO/PVA hydrogel	Sonication, molding via freeze–thaw	0–20	2.2695 kPa^{-1}	0.67/0.84	100	Optimal concentration is 2 mg/mL and tensile strength is 440.213 kPa.	[167]
Carbon ink-coated filter paper	Dip coating	0.1–100	0.0259–0.627 kPa^{-1}	N	4000	N	[169]
PU/G foams	Solvent extraction	0–500	0.05–7.62 kPa^{-1}	0.81/0.81	1000	Optimal graphene content is 30 wt%.	[165]

Material	Fabrication Technique	Sensing Range (kPa)	Sensitivity/Gauge Factor (GF)	Response/ Recovery Time (s)	Durability (Cycles)	Remarks/Comments	Ref
Nitrogen-doped GO, dopamine, and polyaniline composite aerogel	Self-assembly, freeze-drying, and thermal annealing	0–25.48	0.10 kPa^{-1}	N	150	The optimal mass ratio of GO:DA:PANI is 5:2:2, with 1.46% nitrogen.	[166]
P(VDF-TrFE) matrix with MWCNTs	Electrospinning and mechanical drawing	5–50	~540 mV/N	N	N	Self-powered sensor achieved piezoelectric coefficient of 50 pm/V with 98% linearity.	[168]
PDMS/CB/graphene nanosheets	Laser thermoforming	0–100	109.4 kPa^{-1}	0.079/0.055	5000	CB as an endothermic agent and glucose as a porogen.	[170]

Table 6 summarizes 13 carbon-based strain sensors with potential application in food and medical packaging-based monitoring during transportation.

Among the 13 carbon-based strain sensors with potential for application in food and medical packaging-based monitoring during transportation/distribution, CNTs (seven studies) [173–179], rGO (four studies) [167,177,179,180], and graphene (three studies) [181–183] are widely used. These materials were often combined with different highly stretchable and durable polymers or elastomers (e.g., PDMS, PVA, PEI, chitosan, and agar) to improve flexibility and robustness. Several sensors were made of functionalized materials, such as carboxyl-functionalized CNTs [176], polyetherimide-rGO [180], and tannic acid-modified rGO [167], which provided unique features such as self-healing and biocompatibility. Carbon-based strain sensors were generally in the form of layered and 3D composite structures employing hybrid and functionalized materials to enhance sensor performance. Multilayer designs, such as few-layer graphene films [181] has shown to improve sensor sensitivity and mechanical stability. Three-dimensional composites including fragmentized rGO sponge [177] and rGO/MWCNT composites [179] broaden the detection range while also enhancing sensors sensitivity.

Simple and relative cheap methods such as single-step Marangoni self-assembly [182], layer-by-layer assembly [180], sonication [183], and solution casting [175] were used to produce strain sensors which demonstrated low-strain detection (up to 10%) with high sensitivity. Advanced techniques, including microelectromechanical system-assisted electrophoretic deposition (EPD) [173], embedded 3D printing [184], direct writing [179], and screen printing [181] enabled the production of sensors with precise control and broader detection range.

Just for other sensor types, the strain-sensing range varies significantly with material and sensor architecture. The values spanned from 2% in the ultrathin graphene film sensor [182] to 1000% in the carboxyl-functionalized CNTs sensor [176]. Polymer-free CNT sensors fabricated via CVD demonstrated a sensing range of 0–42,100 kPa with high gauge factor (1461), suitable for high-strain applications [174]. Composite sensors' detection range depends on polymers/elastomers flexibility or stretchability as well as the filler concentration. This ranged from 2% for chitosan/graphene [183] to 280% for TA-rGO/PVA [167]. Functionalized materials, such as carboxyl-functionalized CNTs provided high stretchability and self-healing capability, achieving up to 1000% [176]. Layered and network structure CNT/PDMS sensors achieved up to 100% strain [178].

The durability of carbon-based strain sensors varies significantly, from 100 [167] to 10,000 cycles [175]. The CNT/Agar composite sensor was particularly durable, withstanding up to 10,000 cycles, and demonstrated an enhanced strain range and sensitivity due to increased filler concentrations [175]. The TA-rGO/PVA hydrogel strain sensor exhibited quick response and recovery times (670 ms and 840 ms, respectively), but its soft nature limits its durability to 100 cycles [167].

Only four articles [167,175,177,178] reported any response and recovery time and they vary from 20 ms for FGS/AgNPs/SBS composite [177] to 670 ms for TA-rGO/PVA hydrogel sensor [167].

Table 6. Summary of different strain sensors reported in the literature with their fabrication methods and resulting properties including the sensing range, sensitivity, durability, response, and recovery time.

Material	Fabrication Technique	Sensing Range (%)	Sensitivity	Response/ Recovery Time (ms)	Durability (Cycles)	Remarks/Comments	Ref
Patterned MWCNT/PDMS	Microelectromechanical system-assisted EPD	0–14	13–120	N	N	Sensitivity tailored by MWCNT film thickness and entanglement. Sensor adapted to an arbitrarily curve surface.	[173]
Polymer-free CNTs	Hot-wall atmospheric CVD	0–42.1 MPa	1461	N	N	Higher sensitivity in IDE devices than single-gap electrodes.	[174]
CNT/Agar composite	Solution casting	0–118	0.28	160/250	10,000	Increasing filler concentration improved strain from 0.8 to 1.1, and stress from 35.2 to 45.8 kPa.	[175]
PDMS-TDI (2,4′-Tolylene diisocyanate)-carboxyl-functionalized MWCNTs nanocomposite	One-pot synthesis, ultrasonication, and casting	0–1000	0.65–2.43	N	1000	Sensor had 98.1% self-healing efficiency at 60 °C over 9 h.	[176]
Fragmentized rGO sponge (FGS)/AgNPs/polystyrene-butadiene-styrene (SBS) composite	Multiple-step process	0–120	$20.5–1.25 \times 10^7$	20/N	2000	Microcrack contributed to sensitivity. Sensor had 1521 S/cm conductivity and 680% break elongation.	[177]
CNTs/PDMS		0.007–100	87	65/N	1500	Optimal sensor had network cracks and 15 layers of CNT.	[178]
rGO/MWCNTs composite	Direct writing printing	10–40	18.55	N	900	N	[179]
Carbon grease	Embedded 3D printing	400	3.8	N	1000	Up to 10% variation from its original value after large strains.	[184]

Material	Fabrication Technique	Sensing Range (%)	Sensitivity	Response/ Recovery Time (ms)	Durability (Cycles)	Remarks/Comments	Ref
Few-layer graphene	Mechanical exfoliation and screen printing	0–6	20.02	N	100,000 flexing cycles 1000 abrasion cycles	Number of prepared graphene layers was 2–5 layers.	[181]
TA-rGO/PVA hydrogel	Sonication and molding via freeze–thaw cycles	0–280	1.936 78	670/840	100	Optimal concentration is 2 mg/mL and tensile strength is 440.213 kPa.	[167]
PEI-rGO nanocomposite	LBL self-assembly	0–5 (~800 kPa)	N	N	500	Rapid self-healing (~10 s), and 98% efficiency at room temperature.	[180]
Ultrathin graphene film	Single-step Marangoni self-assembly	2	1037	N	N	Optimal thickness is 4.4 nm with 3.4% failure strain.	[182]
Chitosan-graphene	Bath sonication and vacuum filtration	0–2	18.6	N	N	Chitosan-G had better graphene electrical properties than pullulan and alginate.	[183]

3.4. Multifunctional Sensor

Table 7 summarizes 23 carbon-based multifunctional sensors with potential applications in packaging food and medical or pharmaceutical products. Among the studies reviewed, 9 articles examined dual-functional sensors, detecting two stimuli simultaneously [185–193], 11 explored triple-functional sensors [194–204], and 3 quad-functional sensors, focusing on humidity, temperature, pressure, and strain stimuli [205–207]. Graphene, rGO, and CNT-based material were predominantly used, often in combination with different polymers or other materials such as carbon black to enhance the multifunctionality of the sensors. Fabrication methods often involve coating, CVD, molding, and printing, allowing for simple and scalable production. Many sensors incorporated multiple fabrication techniques to optimize performance.

The selective reactivity to specific stimuli was achieved by using different carbon materials or compositions [187,188,190,191,194,203]. For example, Bae et al. (2018) fabricated a dual-mode sensor that utilized SWCNTs/PDMS for pressure sensing (0–25 kPa) and rGO for temperature sensing (22–70 °C) with good sensitivity (0.7/kPa and 0.83%/°C, respectively), quick response (0.05 s and 0.1, respectively), and stability over 10,000 cycles [187]. Similarly, all carbon-based sensors with carbon nanocoils (CNCs) and CNTs for simultaneously sensing temperature, humidity, and strains have been developed by Li et al. [203]. The authors achieved a wide detection range from −266.15 to 126.85 °C (temperature), 10% to 80% (relative humidity) and up to 100% strain with high strain resolution (0.01%) and fast response time (16 ms) alongside a stability of 10,000 cycles. Li et al. [192] developed a dual-mode temperature and strain sensor based on graphene/PEDOT:PSS hydrogel, with a detection range of 7–60 °C for temperature and up to 1000% for strain. The sensor demonstrated high sensitivity (gauge factor 8.1 for strain, −7.16%/°C for temperature), fast response (0.2 s), and stability over 10,000 cycles.

Other reported multiple sensing systems showed a temperature range starting from 20 °C [187–190,193,197,198,202,204–206] or lower pressure range below 0.6 kPa [195,201], limiting their application for packaging when considering the stresses encountered in the transportation/distribution chain.

Table 7. Summary of different multifunctional sensors reported in the literature with their modes, fabrication methods, and resulting properties including the sensing range, sensitivity, durability, response, and recovery time.

No. Modes	Carbon Materials	Modes	Fabrication	Mechanism	Working Range	Sensitivity	Response/ Recovery Time (s)	Durability (Cycles)	Ref
2	Monolayer graphene	Humidity	CVD and oxygen plasma etching	Capacitive Resistive	2–90%RH	17–32%/%RH	~8/~19	1000	[185]
		Temperature		Current	10–90 °C	N	~4/~10	N	
	Cracked paddy-shaped MoS$_2$/graphene foam/Ecoflex	Strain	Thermal CVD, dipping, and annealing	Piezoresistive	0–22%	GF = 24.1	N	N	[186]
		Pressure			0.6–25.4 kPa	3.28–6.06/kPa	N	4000	
	SWCNTs/PDMS	Pressure	Coating and molding	Capacitance	0–25 kPa	0.7/kPa	0.05/N	10,000	[187]
	rGO	Temperature	Spray-coating	Resistive	22–70 °C	0.83%/°C	0.1/N	N	
	PDMS/SWCNT composite	Pressure	Spray coating and leather mold	Piezoresistive	0–400 kPa	0.03–7.76/kPa	0.132/0.12	10,000	[188]
	PDMS/SWCNT composite with thermochromic material	Temperature		Resistive	23–90 °C	N	N	N	
	Graphene–CNT–Silicone adhesive nanocomposite	Humidity	Doctor blade and drop casting	Impedance Capacitance	36–94% RH	−84.5 Ω/%RH 1336.7 pF/%RH	26/74	N	[189]
		Temperature		Impedance	37–87 °C	−19.8 Ω/°C	34/82	N	
	PU@CNT composite	Temperature	Hot pressing	Resistive	30–110 °C	−2.84 × 10^{-3}/°C	N	5000	[190]
	PU dielectric	Pressure		Capacitive	0.1–50 kPa	0.0549/kPa	0.094/0.134	5000	
	GO/SWCNTs/PDMS composite	Humidity	Screen and inkjet printing	Resistive	25–80%RH	0.137–11.145%/%RH	0.5/0.3	N	[191]
	SWCNTs/PDMS composite	Pressure	Blading and doctor blade	Piezoresistive	0.024–230 kPa	27.91–77.78 /kPa	0.03/0.03	6000	
	Graphene/PEDOT:PSS hydrogel	Strain	One-pot method	Resistive	1000%	8.1	0.2/N	10,000	[192]
		Temperature			7–60 °C	−7.16−−0.162%/°C	N	N	

Table 7. *Cont.*

No. Modes	Carbon Materials	Modes	Fabrication	Mechanism	Working Range	Sensitivity	Response/ Recovery Time (s)	Durability (Cycles)	Ref
2	CNTs sponge/PEDOT:PSS/PDMS	Pressure	Soaking and oven drying	Piezoresistive	0–40 kPa	26.8–902.2/kPa	0.063/0.071	500	[193]
		Temperature		Resistive	20–80 °C	0.84%/°C	1.1/1.5	5 days	
3	GO	Humidity	Spray coating	Capacitive	20–90%	0.0589 pF/%RH	N	N	[194]
	rGO	Temperature		Resistive	0–100 °C	−3.4 kΩ/°C	N	N	
	PDMS	Pressure	Lamination	Resistive Capacitive	0–450 kPa	0.002/kPa	0.2/N	2000	
	rGO/CNCs	Compression Strain	Mixing, freezing, freeze-drying, and carbonization	Resistive	0–99%	GF = 369.4	N	10,000	[195]
		Pressure			0.00075 kPa	N	N	N	
		Bending			0.052–180°	N	N	10,000	
	Graphene-glycerol	Strain	Coating	Piezoresistive	0–1000%	GF = 45.13	0.2/0.2	10,000	[196]
		Pressure		Resistive	0–50 kPa	80%	N	N	
		Twisting			0–180°	100%	N	N	
	PDMS-coated microporous polypyrrole/graphene foam (PDMS/PPy/GF)	Pressure	CVD, electrochemical deposition, and dip-coating	Piezoresistive	0–50 kPa	2.01/kPa	0.02/N	10,000	[197]
		Temperature		Thermoelectric	25–70 °C	49.8 µV/K	1.5/8.3	N	
		Strain		Resistive	0–50%	GF = −1.38 (<10%) GF = −0.09 (10–50%)	1/2.5	N	
	Carbon fibers and MWCNTs (CFs-MWCNT) composite	Temperature		Resistive	30–50 °C	1.49–2.46%/°C	N	N	[198]
		Pressure		Piezoresistive	0–60 kPa	0.91–42.5/kPa	0.1/0.1	6000	
		Bending			0–180°	95.5%/rad	N	1000	
	GO-doped-PU nanofiber membrane coated with PEDOT	Pressure	Electrospinning, in situ polymerization, low-temperature oxygen plasma	Piezoresistive	0.001–20 kPa	0.15–20.6/kPa	0.012/N	10,000	[199]
		Strain			0–550%	10.1–193.2	N	10,000	
		Flexion			1.0 cm^{-1}	N	N	6000	

No. Modes	Carbon Materials	Modes	Fabrication	Mechanism	Working Range	Sensitivity	Response/Recovery Time (s)	Durability (Cycles)	Ref
3	CNT/PDMS composite	Pressure / Bending / Tensile strain	Replica molding and ultraviolet-ozone exposure	Piezoresistive	0–270 kPa / 1–6.5 mm / 0–50%	6.67/kPa / 17.7/mm / GF = 409	0.024/0.03 / N / N	10,000 / N / N	[200]
	Nanopapillae-decorated carbon nanosheet (NP-CNS)	Humidity / Strain / Pressure	Pyrolysis and screen printing	Resistive / Piezoresistive	0–96%RH / 0–500% / 0.005–0.6 kPa	8.25 / GF = 21.9–99.9 / N	1.7/100.1 / 0.07/N / 0.032/N	N / N / N	[201]
	rGO/polyorganosiloxane aerogels	Temperature / Pressure / Strain	Copolycondensation	Resistive	20–100 °C / 0.01–110 kPa / 0.1–80%	50.20% / 83.50% / 84%	N / N / N	10,000	[202]
	CNC (10 mg)-CNT (30 mg) buckypaper	Strain	Mixed vacuum filtration and curing	Piezoresistive	0–100%	GF = 352,085	0.033/0.016	10,000	[203]
	Pre-stretched CNC (10 mg)-CNT (80 mg) buckypaper	Temperature	Mixed vacuum filtration, pre-stretch, and curing	Resistive	−266.15–126.85 °C	1.88%/°C	N	10	
	CNC-CNT on cellulose filter paper (1:1)	Humidity	Dripping	Resistive	10–80%RH	N	N	10	
	Graphene woven fabric (GWF)/PDMS composite	Pressure / Strain / Temperature	Catalytic decomposition and dipping	Piezoresistive / Thermoresistive	0–20 kPa / 0–140% / 25–80 °C	0.0142/kPa / GF = 582 / 0.0238/°C	N / N / N	1000 / N / N	[204]
4	CB/rGO composite	Strain / Humidity / Temperature / Pressure	Spray coating	Resistive	N / 16–95%RH / 20–60 °C / 0–250 kPa	GF = 14.6 (compression) GF = 1.8 (tension) / 2.04/%RH / 0.6%/°C / 0.09–0.59%/kPa	~0.34/N / ~300/~80 / ~100/N / ~0.25/N	1000 / N	[205]

<div align="center">**Table 7.** *Cont.*</div>

No. Modes	Carbon Materials	Modes	Fabrication	Mechanism	Working Range	Sensitivity	Response/ Recovery Time (s)	Durability (Cycles)	Ref
4	CB-PDMS	Strain	Spin coating	Resistive	0–40%	GF = 81.2 (0–5%) GF = 28.5 (5–40%)	<0.05/N	4000	[206]
		Pressure			0–20 kPa	4×10^4%	0.1/0.1		
		Flexion			0–150°	N	N	N	
		Temperature			25–150 °C	0.515 ppm/°C	8.4/N		
	Polyaniline-coated MWCNTs	Humidity	Two-step assembly	Conductive	30–80% RH	4.80%	25/38 (Basal layer) 56/55 (double layer)	2500	[207]
		Pressure			0.028–100 kPa	GF = 10			
		Bending strain		Piezoresistive	0–2.7%	GF = 35.8	0.11/0.13	10,000	
		Twisting strain			0–90°	GF = 20.8			

4. Discussion

There is growing research on carbon-based sensors for humidity, temperature, and mechanical stress-monitoring to improve the ability to track food and medical products during transit as illustrated by Figure 3. However, the demand for highly sensitive, durable, and scalable carbon-based sensor technologies is increasing with the global emphasis on real-time logistics monitoring. Challenges persist in translating these sensors from laboratory settings to scalable, commercially viable solutions. This systematic literature review critically assesses the recent advancements in carbon-based sensors designed to monitor humidity, temperature, and mechanical stress, either individually or as part of a multi-stimuli detection system, with potential applications in tracking food and medical products during transit. The performance and reliability of carbon-based sensors are significantly influenced by several factors, including materials selection, structural design, fabrication techniques, electrode configuration, and encapsulation strategy. These factors collectively determine the sensor's sensitivity, responsiveness, durability, and applicability in various transportation environments. A research roadmap developed from the studies (Figure 4) shows some progress over time with efforts toward improving sensing modalities with the integration of different sensing modes as well as enhancing the functionality and properties of the sensing system, for example, with self-healing and lower power consumption or self-powered features. Alongside the need for improving the above-mentioned sensors' performance and features, further investigation and innovations are required especially for sustainable and cost-efficient large-scale production.

The performance and reliability of carbon-based sensors is largely determined by the intrinsic properties and functional requirements of the material used. Among carbon-based materials, GO stands out for humidity sensing (Table 3) due to its low cost, large surface area and high hydrophilicity due to oxygen-containing functional groups which enhance water molecule adsorption capacity and sensitivity. However, excessive oxygen-containing groups can hinder recovery times and compromise long-term stability under high-humidity conditions [208]. Furthermore, drawbacks include potential long-term drift and low selectivity as carbon-based sensors may respond to other gases or contaminants, affecting their specificity toward water vapor.

In contrast, graphene and rGO are better suited for temperature sensors, offering exceptional electrical conductivity, thermal responsiveness, and stability. These properties enable fast response, high sensitivity, and broad detection ranges, making them suitable for most transit conditions for food and medical products including cold chain.

Mechanical sensors use the mechanical strength and piezoresistive properties of graphene for pressure sensing [170], while strain sensors benefit from the flexibility [162], conductivity, and deformation sensitivity of CNTs [173,174,176], rGO [167,177,179], and graphene [181,182]. Nonetheless, these sensors often experience structural instability and poor adhesion to substrates. The combination of GO/MWNT resulted in sensors with 1095-day stability and fast response time (0.061 s) [97]. The combination of these two materials allowed the authors to harness their complementary strengths and help offset each material's individual limitations. Indeed graphene-based sensors typically offer faster response times and greater sensitivity but require careful structural stabilization to maintain long-term stability. In contrast, CNT-based sensors are inherently more stable, but generally exhibit slower response times. Similarly, these carbon-based materials have been used with polymers, such as PDMS [164] or PU [165], which resulted in enhanced flexibility and durability. The evolution of carbon-based sensors has increasingly shifted toward multifunctional sensing platforms, which enable simultaneous detection of multiple stimuli (e.g., pressure, strain, temperature) or analytes (e.g., gases, ions) via distinct response mechanisms, which hold significant potential for smart packaging.
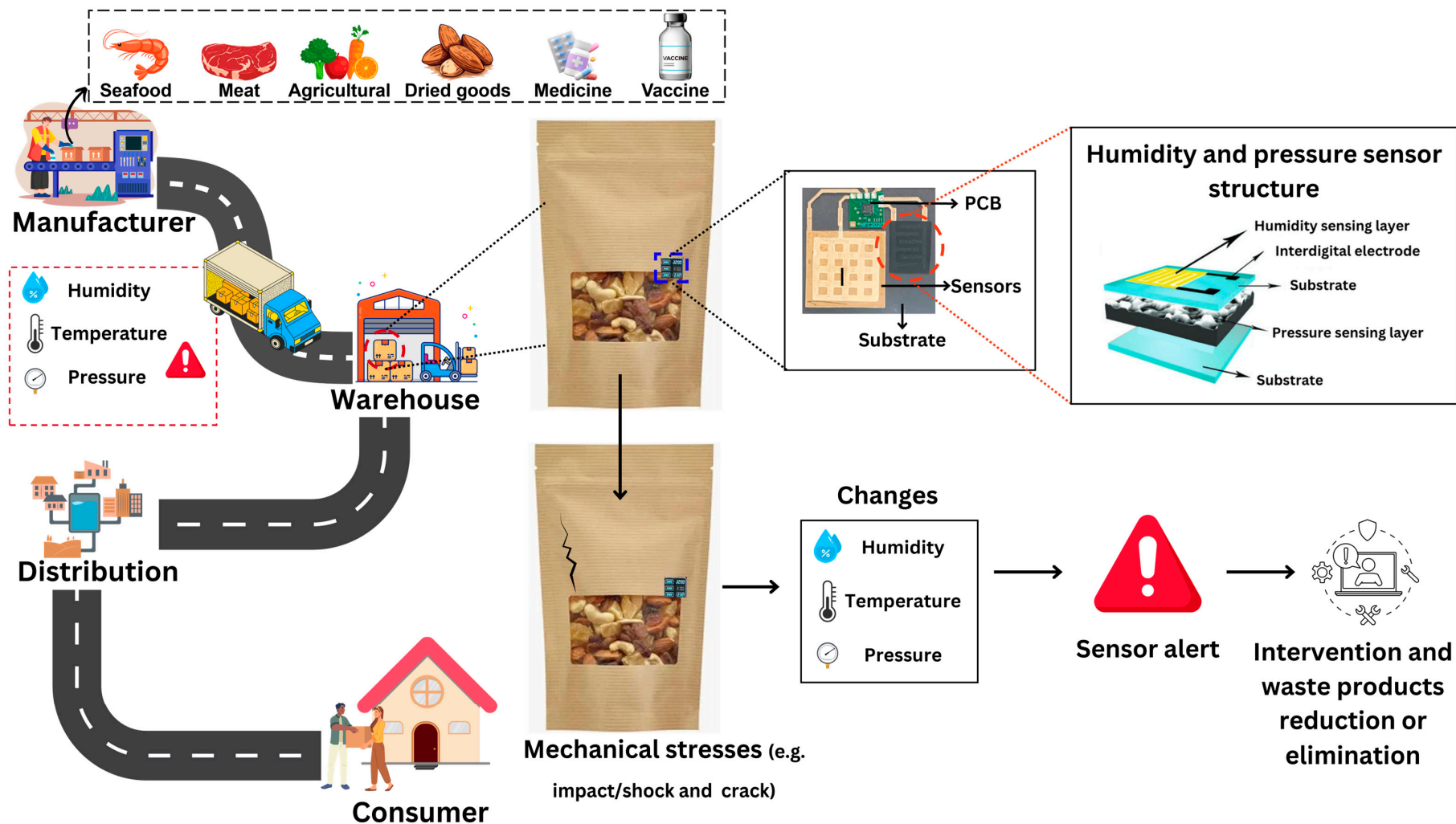
Figure 3. Schematic illustration of packaging with integrated carbon-based sensor systems capable of tracking humidity, temperature, pressure, and mechanical shocks in real time for monitoring food and medical products throughout transportation and storage. As the products transit from the manufacturer to the consumers, sensors continuously record environmental changes and transmit data to the centralized monitoring platforms. When deviations from set thresholds are detected, the system generates immediate alerts, enabling timely interventions and corrective actions.
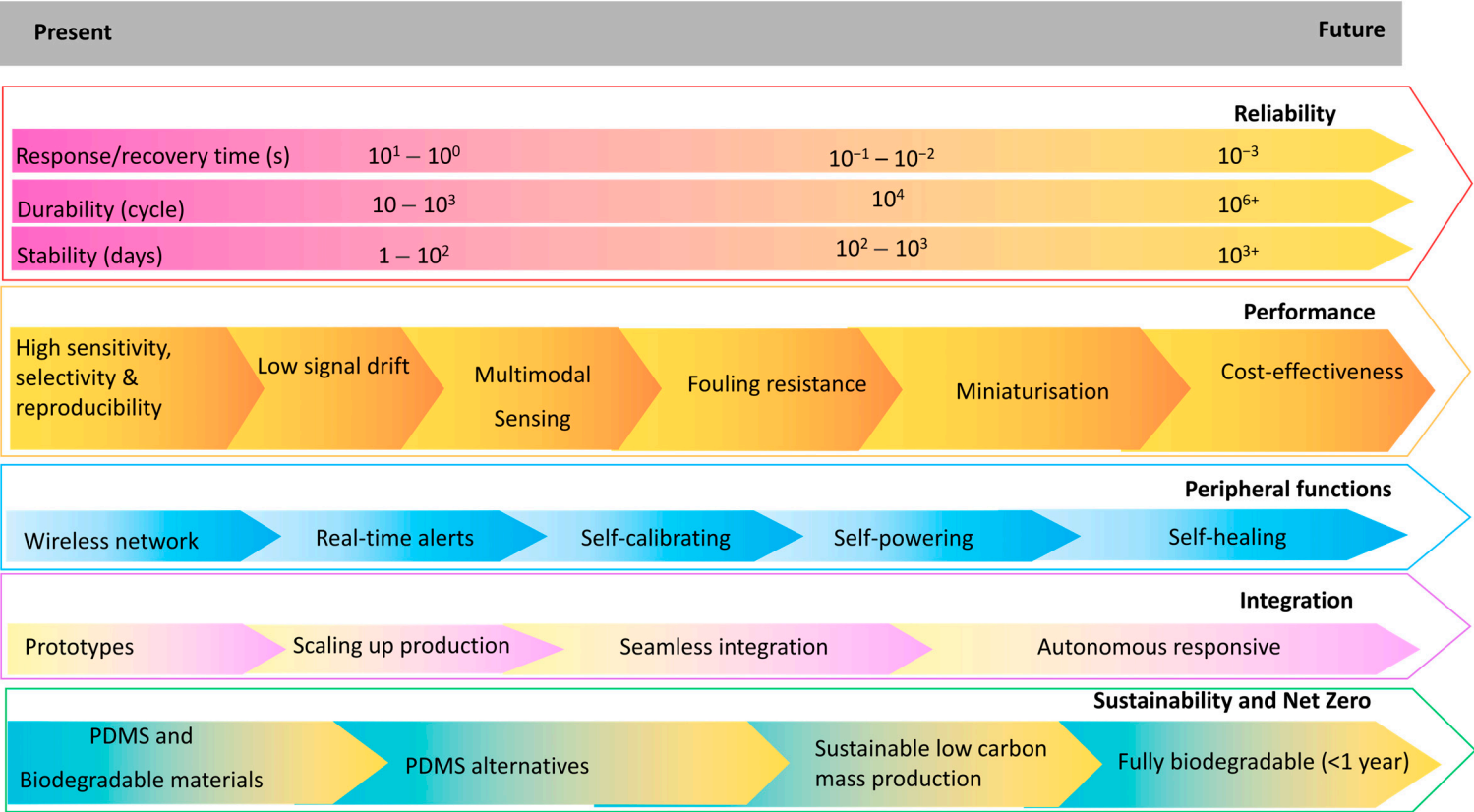
Figure 4. Sensors develop roadmap for smart packaging. The evolution over time is not shown to scale, and each performance and function element is not depicted as a stage of development, but rather as a feature that research is actively progressing toward. Research in the future will focus on improving sensors performance (stability, selectivity, sensitivity, reusability) and sensor integration with different sensing modalities and miniaturized size supported by IoT and AI-driven signal processing for packaging with self-healing, low energy consumption, and self-power function. Although in many publications, durability and stability are estimated by cycling tests, durability refers to the sensor's ability to withstand physical stress, environmental conditions, and wear overtime without degrading, whereas stability is sensor's ability to maintain consistent performance and accuracy over time and, thus, with no drift or changes in sensitivity. However, most research currently focuses on wearable applications, with dual-modal designs prevailing, as adding more sensing modes introduces challenges such as signal interference/decoupling, increased fabrication complexity, and higher costs.

Efforts to overcome these challenges have largely focused on structural design modifications and AI-driven signal processing. Multilayered architectures help minimize signal interference by physically isolating sensing components, though controlling layer thickness and interfacial properties remains a challenge. Ratiometric sensing improves accuracy by analyzing signal ratios instead of absolute values, but its reliability depends on sensor stability and calibration [209]. AI-assisted signal processing enhances detection precision through real-time filtering, noise reduction, and pattern recognition. However, integrating AI introduces challenges such as higher power consumption and computational demands, which must be addressed for practical applications. To transition from prototypes to commercial use, challenges in scalability, durability, and manufacturing must be addressed. Collaboration across materials science, engineering, and AI experts will be key to developing robust, adaptable sensors and sensing systems for real-world deployment.

Nano-structuring carbon materials, such as laser-induced graphene (LIG), graphene flowers, core–shell architectures, and nanoporous structures, have demonstrated significant advantages in sensor applications. The choice between hierarchical (e.g., nanostructured hybrids), hybrid (multi-material composites), or single-element systems (e.g., pure graphene) depends on the sensing targets and operational environments. These materials enhance sensitivity and response time through an increased surface area for the analyte interaction, improved electron transport at defect-engineered interfaces, good mechanical stability, and plasmonic amplification of certain carbon (e.g., graphene quantum dots, porous structure, or hybrid carbon–metal systems) via strong localized surface plasmon resonance effects, thermoplasmonic effects, and charge transfer [128]. The performance enhancements fundamentally stem from the intrinsic link between nanoscale architecture and function. For example, zero-dimensional (0D) quantum dots utilize size-dependent quantum confinement and unique optical properties, making them highly attractive for fluorescence-based sensing and plasmonic enhancement. Whereas one-dimensional (1D) and three-dimensional (3D) structures (e.g., carbon nanotubes, hierarchical porous carbons) leverage strong π–π interactions, offer interconnected diffusion pathways, and enable hierarchical analyte trapping to prevent aggregation, thereby ensuring efficient mass transport. Two-dimensional (2D) structures (e.g., LIG, graphene flowers) prioritize efficient charge transfer and expose abundant edge-reactive sites (such as dangling bonds and oxygenated defects), resulting in rapid binding kinetics. However, while these nanoscale structures provide clear advantages, they also introduce critical challenges. Particles below 20 nm often exhibit aggregation due to high surface energy, which compromises active surface accessibility and surface uniformity, ultimately affecting overall sensor performance [210]. Strategies like vertical alignment (e.g., CNT forests) or 3D carbon frameworks can partially address these challenges by spatially confining nanostructures while retaining their quantum confinement effects or plasmonic properties. Additionally, surface functionalization, template-assisted synthesis, and dispersion control strategies are actively being developed to improve uniformity and long-term stability. Although nanostructured carbon materials demonstrate excellent sensitivity and tunable electronic properties, they face challenges in processing complexity and stability compared to bulk carbon materials. Bulk carbon materials tend to provide higher mechanical integrity and stability, while nano-carbon materials are preferred for high-sensitivity and multifunctional sensing systems. From an economic perspective, the cost of carbon nanomaterials varies significantly due to production complexity, scalability, purity requirements, and applications [211,212]. GO is the most economical due to scalable synthesis, while high purity materials and CVD graphene command premium prices for specialized applications. rGO and MWCNTs offer a balance between cost and performance for conductive composites [212]. However, challenges in maintaining uniformity and quality during upscaling still exist (Figure 5). Advances in

manufacturing technologies are critical to reducing costs and enhancing the scalability for widespread commercial applications. GQDs remain expensive due to low yields and niche use in biomedicine. As manufacturing techniques such as liquid-phase exfoliation, inkjet printing, and low-temperature plasma processes continue to advance, the cost of scalable materials like GO and rGO has stabilized. In the long term, the costs of high-purity carbon nanomaterials (such as CVD graphene and GQDs) are expected to decline with improved synthesis routes and increased market demand.
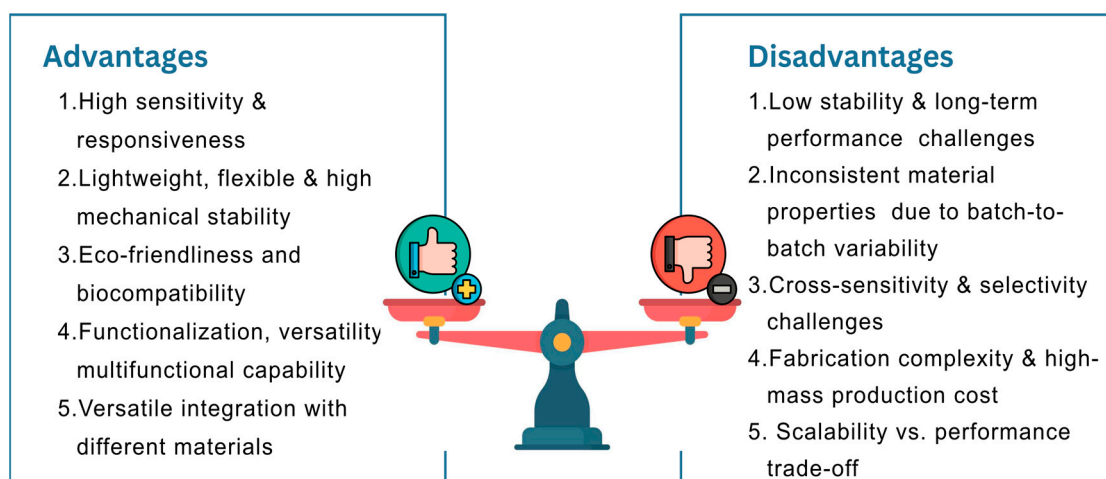
Figure 5. Advantages and disadvantages of carbon-based sensors.

Single-element systems (e.g., pure graphene or CNTs) generally offer simplicity and cost-effectiveness but their limited tunability, low sensitivity and selectivity, and lack of multifunctionality restrict their use. Composites provide a promising and cost-effective approach to overcoming the limitations of single-material sensors by combining carbon materials with other (nano)materials such as polymers, metals or metal oxides, and other carbon additives. Hierarchical and hybrid systems enhance sensor capabilities by increasing surface area, controlling porosity, and optimizing molecular interactions, allowing for greater sensitivity and lower detection limits, while balancing complexity and scalability remains challenging [213]. Silicon polymers, particularly PDMS, are widely used in carbon-based sensors due to their exceptional chemical and thermal stability, biocompatibility, corrosion resistance, flexibility, and ease of fabrication [214]. These properties make PDMS an excellent choice for sensor substrates and encapsulation layers, allowing sensors to sustain large mechanical deformations while maintaining the integrity of the carbon sensing layer. Additionally, its hydrophobicity and chemical inertness protect sensitive materials from environmental factors, enhancing long-term durability. PDMS's adaptability further enables the creation of complex structures and multifunctional sensing platforms. Despite these benefits, PDMS's non-biodegradability poses environmental concerns, particularly in single-use applications, as its crosslinked structure makes recycling challenging [214]. Its fabrication processes also require significant energy or organic solvents [215], increasing its environmental footprint. Technically, achieving uniform carbon dispersion remains a challenge as it results in inappropriate composition, potentially reducing sensor sensitivity and reliability. Future research should explore alternative biodegradable polymers, such as PLA and cellulose derivatives to address these issues.

Recent research trends have highlighted the significant potential of hybrid composites, especially those that incorporate carbon materials with biopolymers, offering a promising balance between performance and sustainability. Cellulose and its derivates, including cellulose nanofiber (CNF) and cellulose nanocrystal (CNC), are promising candidates for

enhancing the performance and sustainability of flexible carbon-based sensors. Cellulose's renewability, biodegradability, and biocompatibility align with sustainability goals and ensure their safety for applications in food and medicine. Its abundant hydroxyl groups and water insolubility enable efficient water molecule adsorption, improving sensitivity and response times of carbon-based humidity sensors [84]. In addition to its role in composite reinforcement, cellulose exhibits a strong nanoscale and microscale response to humidity, which significantly impacts their mechanical properties. For example, a decrease in Young Modulus of cellulosic films with increasing RH values has be reported with CNC films showing smaller reduction, 15.6% (from 10.9 GPa to 9.2 GPa) when compared to other films such as xylan hemicellulose that showed 32.9% reduction (from 7.6 GPa to 5.1 GPa) for a change in relative humidity between 15% and 95% [216]. At the microscale, fiber swelling weakens inter fiber bonding, increasing porosity and reducing tensile strength and elastic modulus, leading to structural instability. While these moisture-induced effects are generally seen as mechanical weaknesses, they are cleverly exploited in paper-based humidity sensors. Humidity-induced cellulose swelling modifies the conductive network of embedded nanomaterials (e.g., carbon nanotubes, graphene oxide), altering electrical resistance or capacitance through nanoparticle separation or dielectric shifts [217]. This phenomenon forms the underpinning mechanism behind the development of sustainable, flexible, and highly responsive paper-based humidity sensors. In this regard, Khan et al., [77] produced a paper cellulose fiber/graphene oxide matrix (PCFGOM) humidity sensor with an increase in response to humidity ranging from 10% to 90% at 1 kHz and 10 kHz, respectively. Although the response time (1.2 s) and recovery time (0.8 s) were relatively good, further study is required as 24 h stability was reported. On the other hand, the mechanical stability of cellulose with carbon-based materials enhances flexibility, responsiveness, and durability of composites, as demonstrated in CNC-GO [64] and CNT-MC [148]. However, cellulose's lower elasticity and stretchability compared to synthetic polymers like PDMS limits its application in mechanical sensors. Modifying cellulose, such as nanofibrillated cellulose [75], polydopamine-coated CNC [64], and methylcellulose (MC) [148], improve its compatibility with hydrophobic carbon materials like graphene, while increasing surface area and hydrophilicity. These modification enable uniform and strong integration with conductive carbon materials via hydrogen bonding or van der Waals interactions, enhancing load transfer and resistance to mechanical deformation and fatigue [75]. Despite these advantages, challenges such as poor sensing results, slow responsiveness, and scalability [77] limited long-term stability [106], and mechanical durability in high humidity or dynamic environments need to be addressed. Future research should focus on tailoring material concentrations, composite structures, and fabrication methods to achieve optimal performance. For example, incorporating ~30 wt% GO in CNF composites has been shown to maximize sensitivity while retaining flexibility [106]. Similarly, a CNT-to-MC ratio of 2:1 enables efficient temperature sensing without compromising mechanical flexibility [148]. Overall, these materials hold great potential for large-scale deployment in packaging sensors and transit monitoring systems, and advancing scalable manufacturing techniques such additive printing could further enhance the viability of these materials for industrial applications.

Fabrication methods significantly influence sensor performance, reproducibility, and industrial scalability. High-precision methods such as CVD produce high-quality films but are costly to consider and are relatively low profit-margin products such as food packaging. It is also energy-intensive, which together limits its large-scale industrial adoption. Solution-based methods such as coating and casting offer scalable and cost-effective alternatives but struggle with uniformity and reproducibility. Emerging approaches such as printing, additive manufacturing, and laser thermoforming enable scalable production,

reducing material waste and allowing geometry customization, but require improvements in precision and production efficiency, especially material viscosity limitations for printing techniques. Achieving consistency, reproducibility, and scalability for large-scale production is a persistent bottleneck. Batch-to-batch variations and resource-intensive methods hinder industrial adoption [170]. Recent progress in machine learning-assisted fabrication and computational tools such as COMSOL Multiphysics 5.5 [74] have shown potential in optimizing spray-coating techniques and 3D-printing processes have enhanced fabrication accuracy and reproducibility, paving the way for scalable, multifunctional sensors.

Future research in carbon-based sensor technology specifically designed for food and medicine or pharmaceutical product packaging in transportation conditions should concentrate on several key areas to enhance sensor performance (stability, sensitivity, and selectivity) scalability and environmental sustainability. These include the development of scalable and eco-friendly fabrication methods, particularly for integrating biodegradable polymers such as PLA and cellulose derivatives with other carbon materials. Material concentrations should be tailored, and composite structures optimized to maximize sensor capabilities and mechanical stability. Hierarchical architectures, hybrid material combinations, and optimized single-element systems could be prioritized to address trade-offs between sensitivity, stability, and manufacturability, especially for multifunctional sensors on a single platform. Additionally, incorporating computational modeling and machine learning-driven optimization can accelerate the design of high-performance sensors. Finally, research should focus on long-term sensor stability under fluctuating humidity and mechanical strain conditions to ensure reliable real-world deployment.

Potential limitations of this review include the qualitative nature of the evaluation. A thematic synthesis based on the type of sensors and production methods was preferred as the variability in the reported approaches to sensor fabrication and the resulting performance metrics could render a meta-analysis impractical.

5. Conclusions

All carbon-based sensors (ACBS) for smart packaging of food and medical/pharmaceutical products are of growing interest, especially from a sustainability point of view. These sensors not only promise to enhance the safety and efficiency of supply chains but also align with increasing regulatory demands for traceability and quality assurance during transit. This review showed that humidity sensors are mainly developed with graphene oxide, whereas graphene and carbon nanotubes are predominantly used for temperature and mechanical (strains and pressure) sensors. Their performance is usually enhanced through engineering composite materials and the selection of appropriate fabrication techniques, which also determine the structural properties of the sensors. Although some progress has been made in developing all carbon-based sensors with biodegradable polymers such as cellulose, PDMS is still largely used in the reported studies, which poses environmental concerns, particularly in single-use applications. Future efforts must prioritize the development of fully biodegradable alternatives or all carbon-based sensors without PDMS with comparable properties. Cellulose and cellulose derivatives appear to be promising materials for green and sustainable sensor development and their sensitivity to moisture should be addressed. Innovations were observed in multifunctional sensor development. However, most research focused on wearable applications with dual-modal designs prevailing. This highlights clear research gaps for extending the work on wearable applications to develop sensing systems with detection ranges that meet the requirements for critical logistics scenarios like deep-frozen vaccine transport (-80 °C to -20 °C) and highly dynamic environments while ensuring scalability. Future research should focus on optimizing

composite composition and structures as well as developing scalable, environmentally friendly fabrication methods to overcome current technical and commercialization barriers.

Promising prospects emerge in four key directions: (1) Sustainable hybrid systems combining biodegradable substrates such as cellulose with bio-derived conductive polymers could enable fully compostable or biodegradable sensors while maintaining performance metrics. (2) Self-healing carbon nanocomposites may revolutionize sensor durability by autonomously repairing mechanical/electrical damage during transit. (3) Integration with emerging technologies, particularly IoT-enabled blockchain tracking, AI-driven predictive analytics, and self-powered systems using triboelectric nanomaterials could transform ACBS into active components of smart logistics networks. (4) Advanced manufacturing paradigms including machine learning-assisted optimization of composite compositions and roll-to-roll manufacturing techniques may bridge the gap between lab-scale prototypes and industrial-scale production. Simultaneously, lifecycle analysis frameworks must be developed to validate the environmental benefits of ACBS against conventional electronic sensors across entire product lifetimes for packaging.

It is anticipated that cross-sector collaboration in material science, green chemistry and engineering, physics, and supply chain digitization would contribute to the next generation of ACBS to achieve parity with conventional electronic sensors within the next decade. This evolution demands a paradigm shift to embracing packaging as an active, intelligent component of food/pharma sustainable logistics ecosystems.

Supplementary Materials: The following supporting information can be downloaded at https://www.mdpi.com/article/10.3390/ma18081862/s1. Table S1: PRISMA Checklist. Ref. [218] is cited in the Supplementary Materials.

Nomenclature

3D	Three-Dimensional
ACBS	All Carbon-Based Sensor
Ag	Silver

BP	Black Phosphorus
CB	Carbon Black
CDs	Carbon Dots
CFs	Carbon Fibers
CMC	Carboxymethyl Cellulose
CNC	Cellulose Nanocrystals
CNCs	Carbon Nanocoils
CNF	Carbon Nanofiber
CNHs	Carbon Nanohorns
CNS	Carbon Nanosheet
CNT−OH	Hydroxyl-functionalized Carbon Nanotubes
CNTs	Carbon Nanotubes
Co_3O_4	Cobalt (II,III) Oxide
CVD	Chemical Vapor Deposition
DA	Dopamine
DLS	Direct Laser-Scribed
EPD	Electrophoretic Deposition
f-rGO	Functionalized Reduced Graphene Oxide
FGS	Fragmentized rGO sponge
G	Graphene
$g\text{-}C_3N_4$	Carbon nitride
GCM	Graphene-coated microfiber
Gcvd	Graphene via Chemical Vapor Deposition
GF	Gauge Factor
GF	Graphene Foam
GNP	Graphene Nanoplatelets
GNRs	Graphene Nanoribbons
GO	Graphene Oxide
GPANI	Polyaniline/Graphene
Gpl	Plasma-Grown Graphene
GQDs	Graphene Quantum Dots
GWF	Graphene Woven Fabrics
HEC	Hydroxyethyl Cellulose
HGO	Hummer's Graphene Oxide
HRGO	Holey-Reduced Graphene Oxide
HSMG	High Strength Metallurgical Graphene
LB	Langmuir-Blodgett
LBL	Layer-by-Layer
LDW	Laser Direct Writing
Li	Lithium
LiCl	Lithium Chloride
LIG	Laser-Induced Graphene
$LiNbO_3$	Lithium Niobate
MC	Methyl Cellulose
Mg	Magnesium
Mn	Manganese
MoS_2	Molybdenum Disulfide
$MoTe_2$	Molybdenum Ditelluride
MWCNT	Multi-Walled Carbon Nanotubes
N	Nitrogen
NFC	Nanofibrillated Cellulose
NP	Nanopapillae
p-AP	p-aminophenol
P(VDF-TrFE)	Poly(Vinylidene Fluoride-Trifluoroethylene)

PAM	Polyacrylamide
PANI	Polyaniline
PCFGOM	Paper Cellulose Fiber/GO Matrix
PDA	Polydopamine
PDMS	Polydimethylsiloxane
PEDOT:PSS	Poly(3,4-ethylenedioxythiophene) Polystyrene Sulfonate
PEG	Polyethylene Glycol
PEI	Polyethyleneimine or Polyetherimide
PHEA	Poly-2-hydroxyethyl acrylate
POS	Polyorganosiloxane
PPy	Polypyrrole
PU	Polyurethane
PVA	Polyvinyl Alcohol
PVB	Polyvinyl Butyral
PVDF	Poly(vinylidene fluoride)
PVP	Poly(vinylpyrrolidone)
QCM	Quartz Crystal Microbalance
rGO	Reduced Graphene Oxide
S	Sulfur
SA	Sodium Alginate
SAO	$SrAl_2O_4$: Eu^{2+}, Dy^{3+}
SBS	Styrene-Butadiene-Styrene
SDBS	Sodium Dodecylbenzenesulfonate
SDC	Shellac-derived Carbon
SDS	Sodium Dodecyl Sulfate
SnO_2	Tin(IV) Oxide
SWCNHs	Single-Walled Carbon Nanohorns
SWCNT	Single-Walled Carbon Nanotubes
TA	Tannic Acid
TDI	2,4'-Tolylene Diisocyanate
TEMPO	2,2,6,6-Tetramethylpiperidine 1-oxyl
TFBG	Tilted Fiber Bragg Grating
TFG	Tilted Fiber Grating
TOCFs	TEMPO-Oxidized Cellulose Fibers
VOCs	Volatile Organic Compounds
WO_3	Tungsten Trioxide
ZnO	Zinc Oxide
ZrO_2	Zirconium Dioxide

References

1. Janik-Karpinska, E.; Brancaleoni, R.; Niemcewicz, M.; Wojtas, W.; Foco, M.; Podogrocki, M.; Bijak, M. Healthcare Waste—A Serious Problem for Global Health. *Healthcare* **2023**, *11*, 242. [CrossRef] [PubMed]
2. Lipinski, B. *SDG TARGET 12.3 ON FOOD LOSS AND WASTE: 2023 PROGRESS REPORT | Champions 12.3*; World Resources Institute: Washington, DC, USA, 2023. Available online: https://champions123.org/publication/sdg-target-123-2023-progress-report (accessed on 21 November 2024).
3. NHS. *NHS Clinical Waste Strategy*; NHS England: London, UK, 2023. Available online: https://www.england.nhs.uk/long-read/nhs-clinical-waste-strategy/ (accessed on 21 November 2024).
4. UKHSA. *Vaccine Incident Guidance: Responding to Errors in Vaccine Storage, Handling and Administration*; UK Health Security Agency: London, UK, 2022. Available online: https://assets.publishing.service.gov.uk/media/62c598188fa8f54e855dfe17/UKHSA-vaccine-incident-guidance-6-july-2022.pdf (accessed on 21 November 2024).
5. WRAP. *Returning to Normality After COVID-19: Food Waste Attitudes and Behaviours in 2021*; WRAP: Banbury, UK, 2021. Available online: https://www.wrap.ngo/sites/default/files/2021-08/food-trends-report-august-2021.pdf (accessed on 21 November 2024).

6.   UNEP. *United Nations Environment Programme Food Waste Index Report 2021*; UNEP: Nairobi, Kenya, 2021. Available online: https://www.unep.org/resources/report/unep-food-waste-index-report-2021 (accessed on 21 November 2024).

7.   *Food Wastage Footprint: Impacts on Natural Resources: Summary Report*; FAO: Rome, Italy, 2013; ISBN 978-92-5-107752-8.

8.   Fortune Business Insights. Smart Packaging Market Size, Share & Industry Analysis, By Technology Type (Modified Atmosphere Packaging (MAP), Active Packaging, and Intelligent Packaging), By Application (Food & Beverages, Personal Care & Cosmetics, Pharmaceuticals, Electronics, E-Commerce, and Others), and Regional Forecast, 2024–2032. 2024. Available online: https://www.fortunebusinessinsights.com/smart-packaging-market-109166 (accessed on 6 November 2024).

9.   Biji, K.B.; Ravishankar, C.N.; Mohan, C.O.; Srinivasa Gopal, T.K. Smart Packaging Systems for Food Applications: A Review. *J. Food Sci. Technol.* **2015**, *52*, 6125–6135. [CrossRef] [PubMed]

10.   Ghaani, M.; Cozzolino, C.A.; Castelli, G.; Farris, S. An Overview of the Intelligent Packaging Technologies in the Food Sector. *Trends Food Sci. Technol.* **2016**, *51*, 1–11. [CrossRef]

11.   Yusufu, D.; Mills, A. A Colourimetric Vacuum Air-Pressure Indicator. *Analyst* **2019**, *144*, 5947–5952. [CrossRef]

12.   Sterr, J.; Fleckenstein, B.S.; Langowski, H.-C. The Effect of High-Pressure Processing on Tray Packages with Modified Atmosphere. *Food Eng. Rev.* **2015**, *7*, 209–221. [CrossRef]

13.   Li, X.; Koh, K.H.; Farhan, M.; Lai, K.W.C. An Ultraflexible Polyurethane Yarn-Based Wearable Strain Sensor with a Polydimethyl-siloxane Infiltrated Multilayer Sheath for Smart Textiles. *Nanoscale* **2020**, *12*, 4110–4118. [CrossRef]

14.   Boz, Z.; Welt, B.A. Permeable Gas Cavity at Elevated Pressure Enhances Modified Atmosphere Packaging of Fresh Produce. *J. Food Sci.* **2018**, *83*, 1639–1649. [CrossRef]

15.   Seo, J.; Li, S.; Tsogbayar, D.; Hwang, T.; Park, J.; Ko, E.; Park, S.-J.; Yang, C.; Lee, H.S. Advanced Multiparallel-Connected Piezoresistive Physical Sensors: Elevating Performance Reliability of Flexible Strain and Pressure Sensors. *ACS Appl. Mater. Interfaces* **2024**, *16*, 22229–22237. [CrossRef]

16.   Bradford, K.J.; Dahal, P.; Van Asbrouck, J.; Kunusoth, K.; Bello, P.; Thompson, J.; Wu, F. The Dry Chain: Reducing Postharvest Losses and Improving Food Safety in Humid Climates. *Trends Food Sci. Technol.* **2018**, *71*, 84–93. [CrossRef]

17.   Kurmanov, N.; Tolysbayev, B.; Abilmazhinov, Y. The Limiting Storage Life of Perishables During Joint Transportation. *CBUP* **2015**, *3*, 499–505. [CrossRef]

18.   WHO. *Good Storage and Distribution Practices*; WHO: Geneva, Switzerland, 2019. Available online: https://www.who.int/publications/i/item/978-92-4-000182-4 (accessed on 13 October 2024).

19.   *ISO 23412:2020*; Indirect, Temperature-Controlled Refrigerated Delivery Services—Land Transport of Parcels with Intermediate Transfer. International Organization for Standardization: Geneva, Switzerland, 2020. Available online: https://www.iso.org/standard/75468.html (accessed on 14 October 2024).

20.   *ISO 23416:2023*; General Specifications and Testing Methods for Temperature-Sensitive Medicinal Packages in Good Distribution Practice Principles. International Organization for Standardization: Geneva, Switzerland, 2023. Available online: https://www.iso.org/obp/ui/#iso:std:iso:23416:ed-1:v1:en (accessed on 14 October 2024).

21.   *ISO 22982-1:2021*; Packaging—Temperature-Controlled Transport Packaging for Parcels—Part 1: General Requirements and Testing Methods. International Organization for Standardization: Geneva, Switzerland, 2021. Available online: https://www.iso.org/standard/74273.html (accessed on 14 October 2024).

22.   *ISO 12048:1994*; Packaging—Complete, Filled Transport Packages—Compression and Stacking Tests. International Organization for Standardization: Geneva, Switzerland, 1994. Available online: https://www.iso.org/standard/21579.html (accessed on 14 October 2024).

23.   *ISO 18602:2013*; Packaging and the Environment—Optimization of the Packaging System. International Organization for Standardization: Geneva, Switzerland, 2013. Available online: https://www.iso.org/standard/55870.html (accessed on 14 October 2024).

24.   *ISO 13355:2016*; Packaging—Complete, Filled Transport Packages and Unit Loads—Vertical Random Vibration Test. International Organization for Standardization: Geneva, Switzerland, 2016. Available online: https://www.iso.org/standard/62098.html (accessed on 14 October 2024).

25.   Tarcan, R.; Todor-Boer, O.; Petrovai, I.; Leordean, C.; Astilean, S.; Botiz, I. Reduced Graphene Oxide Today. *J. Mater. Chem. C* **2020**, *8*, 1198–1224. [CrossRef]

26.   Guo, Y.; Wei, X.; Gao, S.; Yue, W.; Li, Y.; Shen, G. Recent Advances in Carbon Material-Based Multifunctional Sensors and Their Applications in Electronic Skin Systems. *Adv. Funct. Mater.* **2021**, *31*, 2104288. [CrossRef]

27.   Hou, P.-X.; Liu, C.; Cheng, H.-M. Purification of Carbon Nanotubes. *Carbon* **2008**, *46*, 2003–2025. [CrossRef]

28.   Eatemadi, A.; Daraee, H.; Karimkhanloo, H.; Kouhi, M.; Zarghami, N.; Akbarzadeh, A.; Abasi, M.; Hanifehpour, Y.; Joo, S.W. Carbon Nanotubes: Properties, Synthesis, Purification, and Medical Applications. *Nanoscale Res. Lett.* **2014**, *9*, 393. [CrossRef] [PubMed]

29.   Rao, N.; Singh, R.; Bashambu, L. Carbon-Based Nanomaterials: Synthesis and Prospective Applications. *Mater. Today Proc.* **2021**, *44*, 608–614. [CrossRef]

30. Nasir, S.; Hussein, M.; Zainal, Z.; Yusof, N. Carbon-Based Nanomaterials/Allotropes: A Glimpse of Their Synthesis, Properties and Some Applications. *Materials* **2018**, *11*, 295. [CrossRef]

31. Kirchner, E.-M.; Hirsch, T. Recent Developments in Carbon-Based Two-Dimensional Materials: Synthesis and Modification Aspects for Electrochemical Sensors. *Microchim. Acta* **2020**, *187*, 441. [CrossRef]

32. Sevilla, M.; Fuertes, A.B. The Production of Carbon Materials by Hydrothermal Carbonization of Cellulose. *Carbon* **2009**, *47*, 2281–2289. [CrossRef]

33. Simeonova, D.D.; Pollmann, K.; Bianco, A.; Lièvremont, D. Graphene Oxide and Bacteria Interactions: What Is Known and What Should We Expect? *mSphere* **2024**, *9*, e00715-23. [CrossRef]

34. Lv, C.; Hu, C.; Luo, J.; Liu, S.; Qiao, Y.; Zhang, Z.; Song, J.; Shi, Y.; Cai, J.; Watanabe, A. Recent Advances in Graphene-Based Humidity Sensors. *Nanomaterials* **2019**, *9*, 422. [CrossRef]

35. Zhu, S.; Kim, D.; Jeong, C. Recent Development of Mechanical Stimuli Detectable Sensors, Their Future, and Challenges: A Review. *Sensors* **2023**, *23*, 4300. [CrossRef] [PubMed]

36. Mitura, K.; Kornacka, J.; Kopczyńska, E.; Kalisz, J.; Czerwińska, E.; Affeltowicz, M.; Kaczorowski, W.; Kolesińska, B.; Frączyk, J.; Bakalova, T.; et al. Active Carbon-Based Nanomaterials in Food Packaging. *Coatings* **2021**, *11*, 161. [CrossRef]

37. Kamran, U.; Heo, Y.-J.; Lee, J.W.; Park, S.-J. Functionalized Carbon Materials for Electronic Devices: A Review. *Micromachines* **2019**, *10*, 234. [CrossRef] [PubMed]

38. Wang, Y.; Adam, M.L.; Zhao, Y.; Zheng, W.; Gao, L.; Yin, Z.; Zhao, H. Machine Learning-Enhanced Flexible Mechanical Sensing. *Nano-Micro Lett.* **2023**, *15*, 55. [CrossRef]

39. Yang, T.; Jiang, X.; Huang, Y.; Tian, Q.; Zhang, L.; Dai, Z.; Zhu, H. Mechanical Sensors Based on Two-Dimensional Materials: Sensing Mechanisms, Structural Designs and Wearable Applications. *iScience* **2022**, *25*, 103728. [CrossRef]

40. Tang, C.; Wang, Y.; Li, Y.; Zeng, S.; Kong, L.; Li, L.; Sun, J.; Zhu, M.; Deng, T. A Review of Graphene-Based Temperature Sensors. *Microelectron. Eng.* **2023**, *278*, 112015. [CrossRef]

41. European Parliament; Council of the European Union. Regulation (EU) 2025/40 of the European Parliament and of the Council of 19 December 2024 on Packaging and Packaging Waste, Amending Regulation (EU) 2019/1020 and Directive (EU) 2019/904, and Repealing Directive 94/62/EC (Text with EEA Relevance). Available online: http://data.europa.eu/eli/reg/2025/40/oj (accessed on 1 March 2025).

42. European Parliament; Council of the European Union. *European Parliament and Council Directive 94/62/EC of 20 December 1994 on Packaging and Packaging Waste*; Publications Office of the European Union: Luxembourg, 2018; Volume 31994L0062, Available online: http://data.europa.eu/eli/dir/1994/62/oj (accessed on 1 March 2025).

43. Secretary of State for Environment, Food and Rural Affairs. *2024 No. 1332 The Producer Responsibility Obligations (Packaging and Packaging Waste) Regulations 2024*; The Stationery Office: London, UK, 2024. Available online: https://www.legislation.gov.uk/uksi/2024/1332/made (accessed on 1 March 2025).

44. Page, M.J.; McKenzie, J.E.; Bossuyt, P.M.; Boutron, I.; Hoffmann, T.C.; Mulrow, C.D.; Shamseer, L.; Tetzlaff, J.M.; Akl, E.A.; Brennan, S.E.; et al. The PRISMA 2020 Statement: An Updated Guideline for Reporting Systematic Reviews. *Syst. Rev.* **2021**, *10*, 89. [CrossRef]

45. Rathi, K.; Pal, K. Impact of Doping on GO: Fast Response–Recovery Humidity Sensor. *ACS Omega* **2017**, *2*, 842–851. [CrossRef]

46. Fatima, Q.; Haidry, A.A.; Yao, Z.; He, Y.; Li, Z.; Sun, L.; Xie, L. The Critical Role of Hydroxyl Groups in Water Vapor Sensing of Graphene Oxide. *Nanoscale Adv.* **2019**, *1*, 1319–1330. [CrossRef]

47. Serban, B.-C.; Cobianu, C.; Buiu, O.; Bumbac, M.; Dumbravescu, N.; Avramescu, V.; Nicolescu, C.M.; Brezeanu, M.; Radulescu, C.; Craciun, G.; et al. Quaternary Oxidized Carbon Nanohorns—Based Nanohybrid as Sensing Coating for Room Temperature Resistive Humidity Monitoring. *Coatings* **2021**, *11*, 530. [CrossRef]

48. Serban, B.-C.; Cobianu, C.; Buiu, O.; Bumbac, M.; Dumbravescu, N.; Avramescu, V.; Nicolescu, C.M.; Brezeanu, M.; Pachiu, C.; Craciun, G.; et al. Ternary Nanocomposites Based on Oxidized Carbon Nanohorns as Sensing Layers for Room Temperature Resistive Humidity Sensing. *Materials* **2021**, *14*, 2705. [CrossRef] [PubMed]

49. Zhu, J.; Cao, Y.; Chen, H.; Fan, B.; Zou, X.; Cheng, J.; Zhang, C. Rapid-Response Humidity Sensors Based on Ultra-Thin Films Stacked with Single-Layer Graphene Oxide. *Results Chem.* **2024**, *7*, 101444. [CrossRef]

50. Trigona, C.; Al-Hamry, A.; Kanoun, O.; Baglio, S. Analysis of a Hybrid Micro-Electro-Mechanical Sensor Based on Graphene Oxide/Polyvinyl Alcohol for Humidity Measurements. *Sensors* **2019**, *19*, 1720. [CrossRef] [PubMed]

51. Bi, H.; Yin, K.; Xie, X.; Ji, J.; Wan, S.; Sun, L.; Terrones, M.; Dresselhaus, M.S. Ultrahigh Humidity Sensitivity of Graphene Oxide. *Sci. Rep.* **2013**, *3*, 2714. [CrossRef]

52. Li, N.; Chen, X.; Chen, X.; Ding, X.; Zhao, X. Ultrahigh Humidity Sensitivity of Graphene Oxide Combined with Ag Nanoparticles. *RSC Adv.* **2017**, *7*, 45988–45996. [CrossRef]

53. Paterakis, G.; Vaughan, E.; Gawade, D.R.; Murray, R.; Gorgolis, G.; Matsalis, S.; Anagnostopoulos, G.; Buckley, J.L.; O'Flynn, B.; Quinn, A.J.; et al. Highly Sensitive and Ultra-Responsive Humidity Sensors Based on Graphene Oxide Active Layers and High Surface Area Laser-Induced Graphene Electrodes. *Nanomaterials* **2022**, *12*, 2684. [CrossRef]

54. Fei, X.; Huang, J.; Shi, W. Humidity Sensor Composed of Laser-Induced Graphene Electrode and Graphene Oxide for Monitoring Respiration and Skin Moisture. *Sensors* **2023**, *23*, 6784. [CrossRef]

55. Ni, L.; Li, X.; Cai, F.; Dong, Z.; Deng, Y.; Jiang, T.; Su, Z.; Chang, H.; Zhang, Z.; Luo, Y. Printable and Flexible Humidity Sensor Based on Graphene -Oxide-Supported MoTe$_2$ Nanosheets for Multifunctional Applications. *Nanomaterials* **2023**, *13*, 1309. [CrossRef]

56. Priyadharshini, B.; Valsalal, P. An Improved Humidity Sensor with GO-Mn-Doped ZnO Nanocomposite and Dimensional Orchestration of Comb Electrode for Effective Bulk Manufacturing. *Nanomaterials* **2022**, *12*, 1659. [CrossRef]

57. Ganbold, E.; Sharma, P.K.; Kim, E.-S.; Lee, D.-N.; Kim, N.-Y. Capacitive Humidity Sensor with a Rapid Response Time on a GO-Doped P(VDF-TrFE)/LiCl Composite for Noncontact Sensing Applications. *Chemosensors* **2023**, *11*, 122. [CrossRef]

58. Sun, C.; Shi, Q.; Yazici, M.S.; Lee, C.; Liu, Y. Development of a Highly Sensitive Humidity Sensor Based on a Piezoelectric Micromachined Ultrasonic Transducer Array Functionalized with Graphene Oxide Thin Film. *Sensors* **2018**, *18*, 4352. [CrossRef] [PubMed]

59. Yi, R.; Peng, B.; Zhao, Y.; Nie, D.; Chen, L.; Zhang, L. Quartz Crystal Microbalance Humidity Sensors Based on Structured Graphene Oxide Membranes with Magnesium Ions: Design, Mechanism and Performance. *Membranes* **2022**, *12*, 125. [CrossRef] [PubMed]

60. Waheed, W.; Anwer, S.; Khan, M.U.; Sajjad, M.; Alazzam, A. 2D Ti$_3$C$_2$Tx-MXene Nanosheets and Graphene Oxide Based Highly Sensitive Humidity Sensor for Wearable and Flexible Electronics. *Chem. Eng. J.* **2024**, *480*, 147981. [CrossRef]

61. Zeng, S.; Pan, Q.; Huang, Z.; Gu, C.; Wang, T.; Xu, J.; Yan, Z.; Zhao, F.; Li, P.; Tu, Y.; et al. Ultrafast Response of Self-Powered Humidity Sensor of Flexible Graphene Oxide Film. *Mater. Des.* **2023**, *226*, 111683. [CrossRef]

62. Yao, X.; Chen, L.; Luo, Z.; Ye, C.; Liang, F.; Yang, T.; Liu, X.; Tian, X.; Bi, H.; Wang, C.; et al. High-performance Flexible Humidity Sensors for Breath Detection and Non-touch Switches. *Nano Sel.* **2022**, *3*, 1168–1177. [CrossRef]

63. Chen, Q.; Huang, X.; Yao, Y.; Mao, K. Analysis of the Effect of Electrode Materials on the Sensitivity of Quartz Crystal Microbalance. *Nanomaterials* **2022**, *12*, 975. [CrossRef]

64. Yao, Y.; Huang, X.; Chen, Q.; Zhang, Z.; Ling, W. High Sensitivity and High Stability QCM Humidity Sensors Based on Polydopamine Coated Cellulose Nanocrystals/Graphene Oxide Nanocomposite. *Nanomaterials* **2020**, *10*, 2210. [CrossRef]

65. Jiang, B.; Bi, Z.; Hao, Z.; Yuan, Q.; Feng, D.; Zhou, K.; Zhang, L.; Gan, X.; Zhao, J. Graphene Oxide-Deposited Tilted Fiber Grating for Ultrafast Humidity Sensing and Human Breath Monitoring. *Sens. Actuators B Chem.* **2019**, *293*, 336–341. [CrossRef]

66. Syuhada, A.; Shamsudin, M.S.; Daud, S.; Krishnan, G.; Harun, S.W.; Aziz, M.S.A. Single-Mode Modified Tapered Fiber Structure Functionalized With GO-PVA Composite Layer for Relative Humidity Sensing. *Photonic Sens.* **2021**, *11*, 314–324. [CrossRef]

67. Huang, X.; Leng, T.; Georgiou, T.; Abraham, J.; Raveendran Nair, R.; Novoselov, K.S.; Hu, Z. Graphene Oxide Dielectric Permittivity at GHz and Its Applications for Wireless Humidity Sensing. *Sci. Rep.* **2018**, *8*, 43. [CrossRef]

68. Wang, C.; Jiao, C.; Wang, M.; Pan, J.; Wang, Q. GO/CNT−OH/Nafion Nanocomposite Humidity Sensor Based on the LC Wireless Method. *Nanomaterials* **2023**, *13*, 1925. [CrossRef] [PubMed]

69. Alrammouz, R.; Podlecki, J.; Vena, A.; Garcia, R.; Abboud, P.; Habchi, R.; Sorli, B. Highly Porous and Flexible Capacitive Humidity Sensor Based on Self-Assembled Graphene Oxide Sheets on a Paper Substrate. *Sens. Actuators B Chem.* **2019**, *298*, 126892. [CrossRef]

70. Jung, S.I.; Jang, I.R.; Ryu, C.; Park, J.; Padhan, A.M.; Kim, H.J. Graphene Oxide Decorated Multi-Frequency Surface Acoustic Wave Humidity Sensor for Hygienic Applications. *Sci. Rep.* **2023**, *13*, 6838. [CrossRef] [PubMed]

71. Wei, Z.; Huang, J.; Chen, W.; Huang, Q. Fabrication and Characterization of Flexible Capacitive Humidity Sensors Based on Graphene Oxide on Porous PTFE Substrates. *Sensors* **2021**, *21*, 5118. [CrossRef]

72. Wang, X.; Deng, Y.; Chen, X.; Jiang, P.; Cheung, Y.K.; Yu, H. An Ultrafast-Response and Flexible Humidity Sensor for Human Respiration Monitoring and Noncontact Safety Warning. *Microsyst. Nanoeng.* **2021**, *7*, 99. [CrossRef]

73. Ouda, E.; Yousf, N.; Morsy, M.; Duraia, E.-S.M. Flexible Humidity Sensor Based on Light-Scribed Graphene Oxide. *J. Mater. Sci. Mater. Electron.* **2022**, *33*, 18241–18251. [CrossRef]

74. Mohammedture, M.; Al Hashmi, S.; Lu, J.-Y.; Gutierrez, M.; Esawi, A.M.K.; Al Teneiji, M. Numerical Study of a Capacitive Graphene Oxide Humidity Sensor with Etched Configuration. *ACS Omega* **2021**, *6*, 29781–29787. [CrossRef]

75. Yang, Y.; Su, G.; Li, Q.; Zhu, Z.; Liu, S.; Zhuo, B.; Li, X.; Ti, P.; Yuan, Q. Performance of the Highly Sensitive Humidity Sensor Constructed with Nanofibrillated Cellulose/Graphene Oxide/Polydimethylsiloxane Aerogel *via* Freeze Drying. *RSC Adv.* **2021**, *11*, 1543–1552. [CrossRef]

76. Wang, F.; Wang, B.; Zhang, X.; Lu, M.; Zhang, Y.; Sun, C.; Peng, W. High Sensitivity Humidity Detection Based on Functional GO/MWCNTs Hybrid Nano-Materials Coated Titled Fiber Bragg Grating. *Nanomaterials* **2021**, *11*, 1134. [CrossRef]

77. Khan, M.U.; Abbas, Y.; Abunahla, H.; Rezeq, M.; Alazzam, A.; Alamoodi, N.; Mohammad, B. Biocompatible Humidity Sensor Using Paper Cellulose Fiber/GO Matrix for Human Health and Environment Monitoring. *Sens. Actuators B Chem.* **2023**, *393*, 134188. [CrossRef]

78. Khattak, Z.J.; Sajid, M.; Javed, M.; Zeeshan Rizvi, H.M.; Awan, F.S. Mass-Producible 2D Nanocomposite-Based Temperature-Independent All-Printed Relative Humidity Sensor. *ACS Omega* **2022**, *7*, 16605–16615. [CrossRef] [PubMed]

79. Khan, S.A.; Saqib, M.; Rehman, M.M.; Mutee Ur Rehman, H.M.; Rahman, S.A.; Yang, Y.; Kim, S.; Kim, W.-Y. A Full-Range Flexible and Printed Humidity Sensor Based on a Solution-Processed P(VDF-TrFE)/Graphene-Flower Composite. *Nanomaterials* **2021**, *11*, 1915. [CrossRef] [PubMed]

80. Rahman, S.A.; Khan, S.A.; Rehman, M.M.; Kim, W.-Y. Highly Sensitive and Stable Humidity Sensor Based on the Bi-Layered PVA/Graphene Flower Composite Film. *Nanomaterials* **2022**, *12*, 1026. [CrossRef]

81. Saqib, M.; Ali Khan, S.; Mutee Ur Rehman, H.M.; Yang, Y.; Kim, S.; Rehman, M.M.; Young Kim, W. High-Performance Humidity Sensor Based on the Graphene Flower/Zinc Oxide Composite. *Nanomaterials* **2021**, *11*, 242. [CrossRef]

82. Beniwal, A.; Ganguly, P.; Aliyana, A.K.; Khandelwal, G.; Dahiya, R. Screen-Printed Graphene-Carbon Ink Based Disposable Humidity Sensor with Wireless Communication. *Sens. Actuators B Chem.* **2023**, *374*, 132731. [CrossRef]

83. Parthasarathy, P. Graphene/Polypyrrole/Carbon Black Nanocomposite Material Ink-Based Screen-Printed Low-Cost, Flexible Humidity Sensor. *Emergent Mater.* **2023**, *6*, 2053–2060. [CrossRef]

84. Yoshida, A.; Wang, Y.-F.; Tachibana, S.; Hasegawa, A.; Sekine, T.; Takeda, Y.; Hong, J.; Kumaki, D.; Shiba, T.; Tokito, S. Printed, All-Carbon-Based Flexible Humidity Sensor Using a Cellulose Nanofiber/Graphene Nanoplatelet Composite. *Carbon Trends* **2022**, *7*, 100166. [CrossRef]

85. Lim, W.Y.; Goh, C.-H.; Yap, K.Z.; Ramakrishnan, N. One-Step Fabrication of Paper-Based Inkjet-Printed Graphene for Breath Monitor Sensors. *Biosensors* **2023**, *13*, 209. [CrossRef]

86. Wang, H.; Tang, C.; Xu, J. A Highly Sensitive Flexible Humidity Sensor Based on Conductive Tape and a Carboxymethyl Cellulose@graphene Composite. *RSC Adv.* **2023**, *13*, 27746–27755. [CrossRef]

87. Andrić, S.; Tomašević-Ilić, T.; Bošković, M.V.; Sarajlić, M.; Vasiljević-Radović, D.; Smiljanić, M.M.; Spasenović, M. Ultrafast Humidity Sensor Based on Liquid Phase Exfoliated Graphene. *Nanotechnology* **2021**, *32*, 025505. [CrossRef]

88. Lin, W.-D.; Lin, Y.-C.; Wu, R.-J.; Chavali, M. Gr/3D–ZnO Nanocomposites as Humidity Sensors with Enhanced Sensing Response. *Polymers* **2021**, *13*, 1623. [CrossRef] [PubMed]

89. Hernández-Rivera, D.; Rodríguez-Roldán, G.; Mora-Martínez, R.; Suaste-Gómez, E. A Capacitive Humidity Sensor Based on an Electrospun PVDF/Graphene Membrane. *Sensors* **2017**, *17*, 1009. [CrossRef] [PubMed]

90. Phan, D.-T.; Park, I.; Park, A.-R.; Park, C.-M.; Jeon, K.-J. Black P/Graphene Hybrid: A Fast Response Humidity Sensor with Good Reversibility and Stability. *Sci. Rep.* **2017**, *7*, 10561. [CrossRef] [PubMed]

91. Lee, J.-U.; Ma, Y.-W.; Jeong, S.-Y.; Shin, B.-S. Direct Fabrication of Ultra-Sensitive Humidity Sensor Based on Hair-Like Laser-Induced Graphene Patterns. *Micromachines* **2020**, *11*, 476. [CrossRef]

92. Lin, W.-D.; Chang, T.-C.; Wu, R.-J. Humidity Sensors Based on High Performance Graphene/Zirconium Dioxide Nanocomposite Material. *Sens. Mater.* **2018**, *30*, 1297. [CrossRef]

93. Yu, Y.; Zhang, Y.; Jin, L.; Chen, Z.; Li, Y.; Li, Q.; Cao, M.; Che, Y.; Yang, J.; Yao, J. A Fast Response−Recovery 3D Graphene Foam Humidity Sensor for User Interaction. *Sensors* **2018**, *18*, 4337. [CrossRef]

94. Muñoz, R.; León-Boigues, L.; López-Elvira, E.; Munuera, C.; Vázquez, L.; Mompeán, F.; Martín-Gago, J.Á.; Palacio, I.; García-Hernández, M. Acrylates Polymerization on Covalent Plasma-Assisted Functionalized Graphene: A Route to Synthesize Hybrid Functional Materials. *ACS Appl. Mater. Interfaces* **2023**, *15*, 46171–46180. [CrossRef]

95. Shilpa, M.P.; Chethan, B.; Shetty, S.J.; Murari, M.S.; Waikar, M.R.; Sonkawade, R.G.; Gurumurthy, S.C. Highly Responsive Reduced Graphene Oxide Embedded PVDF Flexible Film-Based Room Temperature Operable Humidity Sensor. *Sens. Actuators A Phys.* **2024**, *366*, 115011. [CrossRef]

96. Yang, H.; Ye, Q.; Zeng, R.; Zhang, J.; Yue, L.; Xu, M.; Qiu, Z.-J.; Wu, D. Stable and Fast-Response Capacitive Humidity Sensors Based on a ZnO Nanopowder/PVP-RGO Multilayer. *Sensors* **2017**, *17*, 2415. [CrossRef]

97. Al-Hamry, A.; Lu, T.; Chen, H.; Adiraju, A.; Nasraoui, S.; Brahem, A.; Bajuk-Bogdanović, D.; Weheabby, S.; Pašti, I.A.; Kanoun, O. Ultra-Sensitive and Fast Humidity Sensors Based on Direct Laser-Scribed Graphene Oxide/Carbon Nanotubes Composites. *Nanomaterials* **2023**, *13*, 1473. [CrossRef]

98. Papamatthaiou, S.; Argyropoulos, D.-P.; Farmakis, F.; Georgoulas, N. Investigation of the H_2O Sensing Mechanism of DC-Operated Chemiresistors Based on Graphene Oxide and Thermally Reduced Graphene Oxide. *IEEE Sens. J.* **2019**, *19*, 7841–7848. [CrossRef]

99. Lei, C.; Zhang, J.; Liang, T.; Liu, R.; Zhao, Z.; Xiong, J.; Yin, K. Humidity Sensor Based on rGO-SDS Composite Film. *Micromachines* **2022**, *13*, 504. [CrossRef] [PubMed]

100. Chen, Z.; Wang, Y.; Shang, Y.; Umar, A.; Xie, P.; Qi, Q.; Zhou, G. One-Step Fabrication of Pyranine Modified- Reduced Graphene Oxide with Ultrafast and Ultrahigh Humidity Response. *Sci. Rep.* **2017**, *7*, 2713. [CrossRef]

101. Yan, H.; Chen, Z.; Zeng, L.; Wang, Z.; Zheng, G.; Zhou, R. The Effect of rGO-Doping on the Performance of SnO_2/rGO Flexible Humidity Sensor. *Nanomaterials* **2021**, *11*, 3368. [CrossRef]

102. Kim, S.J.; Park, H.J.; Yoon, E.S.; Choi, B.G. Preparation of Reduced Graphene Oxide Sheets with Large Surface Area and Porous Structure for High-Sensitivity Humidity Sensor. *Chemosensors* **2023**, *11*, 276. [CrossRef]

103. Du, Y.; Li, X.; Zhao, X.; Wang, N.; Li, D. Fabrication and Humidity Sensing of Reduced Graphene Oxide/Polyaniline Composite Film on Flexible Paper Substrate. *Sens. Mater.* **2022**, *34*, 2065. [CrossRef]

104. Müller, C.; Al-Hamry, A.; Kanoun, O.; Rahaman, M.; Zahn, D.R.T.; Matsubara, E.Y.; Rosolen, J.M. Humidity Sensing Behavior of Endohedral Li-Doped and Undoped SWCNT/SDBS Composite Films. *Sensors* **2019**, *19*, 171. [CrossRef]

105. Turkani, V.S.; Maddipatla, D.; Narakathu, B.B.; Saeed, T.S.; Obare, S.O.; Bazuin, B.J.; Atashbar, M.Z. A Highly Sensitive Printed Humidity Sensor Based on a Functionalized MWCNT/HEC Composite for Flexible Electronics Application. *Nanoscale Adv.* **2019**, *1*, 2311–2322. [CrossRef]

106. Zhu, P.; Kuang, Y.; Wei, Y.; Li, F.; Ou, H.; Jiang, F.; Chen, G. Electrostatic Self-Assembly Enabled Flexible Paper-Based Humidity Sensor with High Sensitivity and Superior Durability. *Chem. Eng. J.* **2021**, *404*, 127105. [CrossRef]

107. Arunachalam, S.; Gupta, A.A.; Izquierdo, R.; Nabki, F. Suspended Carbon Nanotubes for Humidity Sensing. *Sensors* **2018**, *18*, 1655. [CrossRef]

108. Lee, Y.; Yoon, J.; Kim, Y.; Kim, D.M.; Kim, D.H.; Choi, S.-J. Humidity Effects According to the Type of Carbon Nanotubes. *IEEE Access* **2021**, *9*, 6810–6816. [CrossRef]

109. Chaloeipote, G.; Samarnwong, J.; Traiwatcharanon, P.; Kerdcharoen, T.; Wongchoosuk, C. High-Performance Resistive Humidity Sensor Based on Ag Nanoparticles Decorated with Graphene Quantum Dots. *R. Soc. Open Sci.* **2021**, *8*, 210407. [CrossRef]

110. Jlassi, K.; Mallick, S.; Eribi, A.; Chehimi, M.M.; Ahmad, Z.; Touati, F.; Krupa, I. Facile Preparation of N-S Co-Doped Graphene Quantum Dots (GQDs) from Graphite Waste for Efficient Humidity Sensing. *Sens. Actuators B Chem.* **2021**, *328*, 129058. [CrossRef]

111. Morsy, M.; Gomaa, I.; Mokhtar, M.M.; ElHaes, H.; Ibrahim, M. Design and Implementation of Humidity Sensor Based on Carbon Nitride Modified with Graphene Quantum Dots. *Sci. Rep.* **2023**, *13*, 2891. [CrossRef] [PubMed]

112. Wu, J.; Yin, C.; Zhou, J.; Li, H.; Liu, Y.; Shen, Y.; Garner, S.; Fu, Y.; Duan, H. Ultra-Thin Glass Based Flexible, Transparent and Ultra-Sensitive Surface Acoustic Wave Humidity Sensor with ZnO Nanowires and Graphene Quantum Dots. *ACS Appl. Mater. Interfaces* **2020**, *12*, 39817–39825. [CrossRef]

113. Joshi, S.R.; Kim, B.; Kim, S.-K.; Kim, G.-H.; Song, W.; Park, K.; Shin, H. Low-Cost and Fast-Response Resistive Humidity Sensor Comprising Biopolymer-Derived Carbon Thin Film and Carbon Microelectrodes. *J. Electrochem. Soc.* **2020**, *167*, 147511. [CrossRef]

114. Ling, T.Y.; Pu, S.H.; Fishlock, S.J.; Han, Y.; Reynolds, J.D.; McBride, J.W.; Chong, H.M.H. Sensing Performance of Nanocrystalline Graphite-Based Humidity Sensors. *IEEE Sens. J.* **2019**, *19*, 5421–5428. [CrossRef]

115. Serban, B.C.; Buiu, O.; Dumbravescu, N.; Cobianu, C.; Avramescu, V.; Brezeanu, M.; Bumbac, M.; Nicolescu, C.M. Oxidized Carbon Nanohorns as Novel Sensing Layer for Resistive Humidity Sensor. *ACSi* **2020**, *67*, 469–475. [CrossRef]

116. Saquib, M.; Shiraj, S.; Nayak, R.; Nirmale, A.; Selvakumar, M. Synthesis and Fabrication of Graphite/WO$_3$ Nanocomposite-Based Screen-Printed Flexible Humidity Sensor. *J. Electron. Mater.* **2023**, *52*, 4226–4238. [CrossRef]

117. Koskinen, T.; Juntunen, T.; Tittonen, I. Large-Area Thermal Distribution Sensor Based on Multilayer Graphene Ink. *Sensors* **2020**, *20*, 5188. [CrossRef]

118. Wang, S.; Feng, M.; Wu, S.; Wang, Q.; Zhang, L. Highly Sensitive Temperature Sensor Based on Gain Competition Mechanism Using Graphene Coated Microfiber. *IEEE Photonics J.* **2018**, *10*, 1–8. [CrossRef]

119. Pan, J.; Liu, S.; Zhang, H.; Lu, J. A Flexible Temperature Sensor Array with Polyaniline/Graphene–Polyvinyl Butyral Thin Film. *Sensors* **2019**, *19*, 4105. [CrossRef] [PubMed]

120. Landi, G.; Granata, V.; Germano, R.; Pagano, S.; Barone, C. Low-Power and Eco-Friendly Temperature Sensor Based on Gelatin Nanocomposite. *Nanomaterials* **2022**, *12*, 2227. [CrossRef]

121. Landi, G.; Pagano, S.; Granata, V.; Avallone, G.; La Notte, L.; Palma, A.L.; Sdringola, P.; Puglisi, G.; Barone, C. Regeneration and Long-Term Stability of a Low-Power Eco-Friendly Temperature Sensor Based on a Hydrogel Nanocomposite. *Nanomaterials* **2024**, *14*, 283. [CrossRef]

122. Jasmi, F.; Azeman, N.H.; Bakar, A.A.A.; Zan, M.S.D.; Haji Badri, K.; Su'ait, M.S. Ionic Conductive Polyurethane-Graphene Nanocomposite for Performance Enhancement of Optical Fiber Bragg Grating Temperature Sensor. *IEEE Access* **2018**, *6*, 47355–47363. [CrossRef]

123. Štulík, J.; Musil, O.; Josefík, F.; Kadlec, P. Graphene-Based Temperature Sensors–Comparison of the Temperature and Humidity Dependences. *Nanomaterials* **2022**, *12*, 1594. [CrossRef]

124. Gong, X.; Zhang, L.; Huang, Y.; Wang, S.; Pan, G.; Li, L. Directly Writing Flexible Temperature Sensor with Graphene Nanoribbons for Disposable Healthcare Devices. *RSC Adv.* **2020**, *10*, 22222–22229. [CrossRef]

125. Chen, X.; Zhang, R.; Wan, Z.; Wu, Z.; Song, D.; Xiao, X. Laser-Induced Graphene Based Flexible Sensing and Heating for Food Monitoring. *ACS Appl. Electron. Mater.* **2024**, *6*, 3597–3609. [CrossRef]

126. Li, Q.; Bai, R.; Guo, L.; Gao, Y. All Laser Direct Writing Process for Temperature Sensor Based on Graphene and Silver. *Front. Optoelectron.* **2024**, *17*, 5. [CrossRef]

127. Davaji, B.; Cho, H.D.; Malakoutian, M.; Lee, J.-K.; Panin, G.; Kang, T.W.; Lee, C.H. A Patterned Single Layer Graphene Resistance Temperature Sensor. *Sci. Rep.* **2017**, *7*, 8811. [CrossRef]

128. Irfan, M.; Khan, Y.; Rehman, A.U.; Butt, M.A.; Khonina, S.N.; Kazanskiy, N.L. Plasmonic Refractive Index and Temperature Sensor Based on Graphene and LiNbO$_3$. *Sensors* **2022**, *22*, 7790. [CrossRef] [PubMed]

129. Viti, L.; Riccardi, E.; Beere, H.E.; Ritchie, D.A.; Vitiello, M.S. Real-Time Measure of the Lattice Temperature of a Semiconductor Heterostructure Laser via an On-Chip Integrated Graphene Thermometer. *ACS Nano* **2023**, *17*, 6103–6112. [CrossRef] [PubMed]

130. Lei, S.; Su, N.; Li, M. Thermal-Resistance Effect of Graphene at High Temperatures in Nanoelectromechanical Temperature Sensors. *Micromachines* **2022**, *13*, 2078. [CrossRef] [PubMed]

131. Han, S.; Zhou, S.; Mei, L.; Guo, M.; Zhang, H.; Li, Q.; Zhang, S.; Niu, Y.; Zhuang, Y.; Geng, W.; et al. Nanoelectromechanical Temperature Sensor Based on Piezoresistive Properties of Suspended Graphene Film. *Nanomaterials* **2023**, *13*, 1103. [CrossRef]

132. Wang, J.; Wang, Y.; Su, N.; Li, M. Improving Consistency and Performance of Graphene-Based Devices via Al Sacrificial Layer. *Colloid Interface Sci. Commun.* **2023**, *56*, 100743. [CrossRef]

133. Pawlak, R.; Lebioda, M.; Rymaszewski, J.; Szymanski, W.; Kolodziejczyk, L.; Kula, P. A Fully Transparent Flexible Sensor for Cryogenic Temperatures Based on High Strength Metallurgical Graphene. *Sensors* **2016**, *17*, 51. [CrossRef]

134. Kun, H.; Bin, L.; Orban, M.; Donghai, Q.; Hongbo, Y. Accurate Flexible Temperature Sensor Based on Laser-Induced Graphene Material. *Shock Vib.* **2021**, *2021*, 9938010. [CrossRef]

135. Fernández Sánchez-Romate, X.X.; Del Bosque García, A.; Sánchez, M.; Ureña, A. Electrical Transport Mechanisms in Graphene Nanoplatelet Doped Polydimethylsiloxane and Application to Ultrasensitive Temperature Sensors. *ACS Appl. Mater. Interfaces* **2023**, *15*, 22377–22394. [CrossRef]

136. Liu, G.; Tan, Q.; Kou, H.; Zhang, L.; Wang, J.; Lv, W.; Dong, H.; Xiong, J. A Flexible Temperature Sensor Based on Reduced Graphene Oxide for Robot Skin Used in Internet of Things. *Sensors* **2018**, *18*, 1400. [CrossRef]

137. Sehrawat, P.; Abid; Islam, S.S.; Mishra, P. Reduced Graphene Oxide Based Temperature Sensor: Extraordinary Performance Governed by Lattice Dynamics Assisted Carrier Transport. *Sens. Actuators B Chem.* **2018**, *258*, 424–435. [CrossRef]

138. Neella, N.; Gaddam, V.; Nayak, M.M.; Dinesh, N.S.; Rajanna, K. Scalable Fabrication of Highly Sensitive Flexible Temperature Sensors Based on Silver Nanoparticles Coated Reduced Graphene Oxide Nanocomposite Thin Films. *Sens. Actuators A Phys.* **2017**, *268*, 173–182. [CrossRef]

139. Barmpakos, D.; Belessi, V.; Schelwald, R.; Kaltsas, G. Evaluation of Inkjet-Printed Reduced and Functionalized Water-Dispersible Graphene Oxide and Graphene on Polymer Substrate—Application to Printed Temperature Sensors. *Nanomaterials* **2021**, *11*, 2025. [CrossRef] [PubMed]

140. Khan, J.; Mariatti, M.; Zubir, S.A.; Rusli, A.; Manaf, A.A.; Khirotdin, R.K. Eco-Friendly Alkali Lignin-Assisted Water-Based Graphene Oxide Ink and Its Application as a Resistive Temperature Sensor. *Nanotechnology* **2024**, *35*, 055301. [CrossRef] [PubMed]

141. Niu, Y.; Han, Y.; Cheng, H.; Xiong, Z.; Luo, B.; Ma, T.; Li, L.; Liu, S.; Chen, X.; Yi, C. Synthesized Silver Nanoparticles Decorated Reduced Graphene Oxide/Silver Ink for Aerosol Jet Printed Conformal Temperature Sensor with a Wide Sensing Range and Excellent Stability. *J. Mater. Res. Technol.* **2023**, *25*, 873–886. [CrossRef]

142. Sehrawat, P.; Abid, A.; Islam, S.S. An Ultrafast Quantum Thermometer from Graphene Quantum Dots. *Nanoscale Adv.* **2019**, *1*, 1772–1783. [CrossRef]

143. Liu, Q.; Tai, H.; Yuan, Z.; Zhou, Y.; Su, Y.; Jiang, Y. A High-Performances Flexible Temperature Sensor Composed of Polyethyleneimine/Reduced Graphene Oxide Bilayer for Real-Time Monitoring. *Adv. Mater. Technol.* **2019**, *4*, 1800594. [CrossRef]

144. Xie, Z.; Li, H.; Mi, H.-Y.; Feng, P.-Y.; Liu, Y.; Jing, X. Freezing-Tolerant, Widely Detectable and Ultra-Sensitive Composite Organohydrogel for Multiple Sensing Applications. *J. Mater. Chem. C* **2021**, *9*, 10127–10137. [CrossRef]

145. Morsy, M.; Darwish, A.G.; Mokhtar, M.M.; Elbashar, Y.; Elzwawy, A. Preparation, Investigation, and Temperature Sensing Application of rGO/SnO$_2$/Co$_3$O$_4$ Composite. *J. Mater. Sci. Mater. Electron.* **2022**, *33*, 25419–25433. [CrossRef]

146. Kumar, A.; Hsieh, P.-Y.; Shaikh, M.O.; Kumar, R.K.R.; Chuang, C.-H. Flexible Temperature Sensor Utilizing MWCNT Doped PEG-PU Copolymer Nanocomposites. *Micromachines* **2022**, *13*, 197. [CrossRef]

147. Tsai, T.-W.; Ni, I.-C.; Wu, C.-I.; Cheng, I.-C.; Chen, J.-Z. Effect of Solution Aging on Temperature Sensitivity of CNT/PEDOT:PSS. *ECS J. Solid State Sci. Technol.* **2023**, *12*, 027001. [CrossRef]

148. Xiao, Y.; Lin, J.; Xiao, J.; Weng, M.; Zhang, W.; Zhou, P.; Luo, Z.; Chen, L. A Multi-Functional Light-Driven Actuator with an Integrated Temperature-Sensing Function Based on a Carbon Nanotube Composite. *Nanoscale* **2021**, *13*, 6259–6265. [CrossRef] [PubMed]

149. Turkani, V.S.; Maddipatla, D.; Narakathu, B.B.; Bazuin, B.J.; Atashbar, M.Z. A Carbon Nanotube Based NTC Thermistor Using Additive Print Manufacturing Processes. *Sens. Actuators A Phys.* **2018**, *279*, 1–9. [CrossRef]

150. Kuzubasoglu, B.A.; Sayar, E.; Bahadir, S.K. Inkjet-Printed CNT/PEDOT:PSS Temperature Sensor on a Textile Substrate for Wearable Intelligent Systems. *IEEE Sens. J.* **2021**, *21*, 13090–13097. [CrossRef]

151. Ben-Shimon, Y.; Ya'akobovitz, A. Flexible and Bio-Compatible Temperature Sensors Based on Carbon Nanotube Composites. *Measurement* **2021**, *172*, 108889. [CrossRef]

152. Song, H.; Zhang, Y.; Cao, J. Sensing Mechanism of an Ionization Gas Temperature Sensor Based on a Carbon Nanotube Film. *RSC Adv.* **2017**, *7*, 53265–53269. [CrossRef]

153. Sarma, S.; Lee, J.H. Developing Efficient Thin Film Temperature Sensors Utilizing Layered Carbon Nanotube Films. *Sensors* **2018**, *18*, 3182. [CrossRef]

154. Yang, H.; Qi, D.; Liu, Z.; Chandran, B.K.; Wang, T.; Yu, J.; Chen, X. Soft Thermal Sensor with Mechanical Adaptability. *Adv. Mater.* **2016**, *28*, 9175–9181. [CrossRef]

155. Leng, X.; Li, W.; Luo, D.; Wang, F. Differential Structure With Graphene Oxide for Both Humidity and Temperature Sensing. *IEEE Sens. J.* **2017**, *17*, 4357–4364. [CrossRef]

156. Cai, C.; Qin, M. High-performance Bulk Silicon Interdigital Capacitive Temperature Sensor Based on Graphene Oxide. *Electron. lett.* **2013**, *49*, 488–490. [CrossRef]

157. Soni, M.; Bhattacharjee, M.; Ntagios, M.; Dahiya, R. Printed Temperature Sensor Based on PEDOT: PSS-Graphene Oxide Composite. *IEEE Sens. J.* **2020**, *20*, 7525–7531. [CrossRef]

158. Zhou, C.; Tang, N.; Zhang, X.; Fang, Y.; Jiang, Y.; Zhang, H.; Duan, X. Simultaneously Optimize the Response Speed and Sensitivity of Low Dimension Conductive Polymers for Epidermal Temperature Sensing Applications. *Front. Chem.* **2020**, *8*, 194. [CrossRef] [PubMed]

159. Zhao, Y.; Tong, R.-J.; Chen, M.-Q.; Xia, F. Fluorescence Temperature Sensor Based on GQDs Solution Encapsulated in Hollow Core Fiber. *IEEE Photon. Technol. Lett.* **2017**, *29*, 1544–1547. [CrossRef]

160. Zhang, L.; Lyu, S.; Zhang, Q.; Wu, Y.; Melcher, C.; Chmely, S.C.; Chen, Z.; Wang, S. Dual-Emitting Film with Cellulose Nanocrystal-Assisted Carbon Dots Grafted $SrAl_2O_4$, Eu^{2+}, Dy^{3+} Phosphors for Temperature Sensing. *Carbohydr. Polym.* **2019**, *206*, 767–777. [CrossRef]

161. Zhang, Q.; Liang, X.; Bi, W.; Pang, X.; Zhao, Y. Integrated Amorphous Carbon Film Temperature Sensor with Silicon Accelerometer into MEMS Sensor. *Micromachines* **2024**, *15*, 1144. [CrossRef]

162. Smith, A.D.; Niklaus, F.; Paussa, A.; Schröder, S.; Fischer, A.C.; Sterner, M.; Wagner, S.; Vaziri, S.; Forsberg, F.; Esseni, D.; et al. Piezoresistive Properties of Suspended Graphene Membranes under Uniaxial and Biaxial Strain in Nanoelectromechanical Pressure Sensors. *ACS Nano* **2016**, *10*, 9879–9886. [CrossRef]

163. Wang, J.; Zhu, Z.; Qi, Y.; Li, M. A Novel Crossbeam Structure with Graphene Sensing Element for N/MEMS Mechanical Sensors. *Nanomaterials* **2022**, *12*, 2101. [CrossRef]

164. Kou, H.; Zhang, L.; Tan, Q.; Liu, G.; Dong, H.; Zhang, W.; Xiong, J. Wireless Wide-Range Pressure Sensor Based on Graphene/PDMS Sponge for Tactile Monitoring. *Sci. Rep.* **2019**, *9*, 3916. [CrossRef]

165. Feng, C.; Yi, Z.; Jin, X.; Seraji, S.M.; Dong, Y.; Kong, L.; Salim, N. Solvent Crystallization-Induced Porous Polyurethane/Graphene Composite Foams for Pressure Sensing. *Compos. Part B Eng.* **2020**, *194*, 108065. [CrossRef]

166. Deng, Z.; Gao, C.; Feng, S.; Zhang, H.; Liu, Y.; Zhu, Y.; Wang, J.; Xiang, X.; Xie, H. Highly Compressible, Light-Weight and Robust Nitrogen-Doped Graphene Composite Aerogel for Sensitive Pressure Sensors. *Chem. Eng. J.* **2023**, *471*, 144790. [CrossRef]

167. Du, B.; Chao, Y.; Yang, K.; Li, B.; Luo, R.; Zhou, S.; Li, H. Stretchable and Tough Tannic Acid-Modified Graphene Oxide/Polyvinyl Alcohol Conductive Hydrogels for Strain and Pressure Sensors. *AIP Adv.* **2022**, *12*, 095206. [CrossRef]

168. Wang, A.; Hu, M.; Zhou, L.; Qiang, X. Self-Powered Wearable Pressure Sensors with Enhanced Piezoelectric Properties of Aligned P(VDF-TrFE)/MWCNT Composites for Monitoring Human Physiological and Muscle Motion Signs. *Nanomaterials* **2018**, *8*, 1021. [CrossRef] [PubMed]

169. Feng, X.; Ran, Y.; Li, X.; Xu, H.; Huang, Q.; Duan, Z.; Yuan, Z.; Jiang, Y.; Tai, H. Amorphous Carbon Derived from Daily Carbon Ink for Wide Detection Range, Low-Cost, Eco-Friendly and Flexible Pressure Sensor. *Mater. Chem. Phys.* **2024**, *321*, 129489. [CrossRef]

170. Guo, D.; Lei, X.; Chen, H.; Yi, L.; Li, Y.; Zhao, Y.; Liu, F.; Cheng, G.J. Highly Flexible and Sensitive Pressure Sensor: Fabrication of Porous PDMS/Graphene Composite via Laser Thermoforming. *Adv. Sens. Res.* **2024**, *3*, 2300165. [CrossRef]

171. Park, S.W.; Das, P.S.; Park, J.Y. Development of Wearable and Flexible Insole Type Capacitive Pressure Sensor for Continuous Gait Signal Analysis. *Org. Electron.* **2018**, *53*, 213–220. [CrossRef]

172. Marshall, J.E.; Zhenova, A.; Roberts, S.; Petchey, T.; Zhu, P.; Dancer, C.E.J.; McElroy, C.R.; Kendrick, E.; Goodship, V. On the Solubility and Stability of Polyvinylidene Fluoride. *Polymers* **2021**, *13*, 1354. [CrossRef]

173. Xu, W.; Allen, M.G. Deformable Strain Sensors Based on Patterned MWCNTs/Polydimethylsiloxane Composites. *J. Polym. Sci. B Polym. Phys.* **2013**, *51*, 1505–1512. [CrossRef]

174. Chang, W.-T.; Yang, F.-S. Extended Width in Discontinuously Connected Polymer-Free Carbon Nanotubes Grown between Electrodes. *Phys. B Condens. Matter* **2015**, *459*, 24–28. [CrossRef]

175. Tippo, P.; Maruthappan, M.; Ručman, S.; Jumrus, N.; Kantarak, E.; Sroila, W.; Thongsuwan, W.; Wiranwetchayan, O.; Thongpan, W.; Kumpika, T.; et al. Processing Improvement of Response and Stability of Strain Sensor Based on CNT-bioplastic Composite for Estimation of Elbow Angles. *J. Appl. Polym. Sci.* **2024**, *141*, e55892. [CrossRef]

176. Jing, X.; Ma, Z.; Antwi-Afari, M.F.; Wang, L.; Li, H.; Mi, H.-Y.; Feng, P.-Y.; Liu, Y. Synthesis and Fabrication of Supramolecular Polydimethylsiloxane-Based Nanocomposite Elastomer for Versatile and Intelligent Sensing. *Ind. Eng. Chem. Res.* **2021**, *60*, 10419–10430. [CrossRef]

177. Zhao, S.; Guo, L.; Li, J.; Li, N.; Zhang, G.; Gao, Y.; Li, J.; Cao, D.; Wang, W.; Jin, Y.; et al. Binary Synergistic Sensitivity Strengthening of Bioinspired Hierarchical Architectures Based on Fragmentized Reduced Graphene Oxide Sponge and Silver Nanoparticles for Strain Sensors and Beyond. *Small* **2017**, *13*, 1700944. [CrossRef]

178. Wang, S.; Xiao, P.; Liang, Y.; Zhang, J.; Huang, Y.; Wu, S.; Kuo, S.-W.; Chen, T. Network Cracks-Based Wearable Strain Sensors for Subtle and Large Strain Detection of Human Motions. *J. Mater. Chem. C* **2018**, *6*, 5140–5147. [CrossRef]

179. Chen, C.; Chu, F.; Zhang, Y.; Ma, M.; Sun, R.; Jia, P.; Sun, J. Fabricating Flexible Strain Sensor with Direct Writing Graphene/Carbon Nanotube Aerogel. *ACS Appl. Electron. Mater.* **2023**, *5*, 1429–1436. [CrossRef]

180. Yao, Y.; Tai, H.; Wang, D.; Jiang, Y.; Yuan, Z.; Zheng, Y. One-Pot Preparation and Applications of Self-Healing, Self-Adhesive PAA-PDMS Elastomers. *J. Semicond.* **2019**, *40*, 112602. [CrossRef]

181. Zhang, Y.; Lin, H.; Zhang, L.; Peng, S.; Weng, Z.; Wang, J.; Wu, L.; Zheng, L. Mechanical Exfoliation Assisted with Carbon Nanospheres to Prepare a Few-Layer Graphene for Flexible Strain Sensor. *Appl. Surf. Sci.* **2023**, *611*, 155649. [CrossRef]

182. Li, X.; Yang, T.; Yang, Y.; Zhu, J.; Li, L.; Alam, F.E.; Li, X.; Wang, K.; Cheng, H.; Lin, C.-T.; et al. Large-Area Ultrathin Graphene Films by Single-Step Marangoni Self-Assembly for Highly Sensitive Strain Sensing Application. *Adv. Funct. Mater.* **2016**, *26*, 1322–1329. [CrossRef]

183. Kasim, N.F.A.; Idris, W.F.W.; Abdullah, A.H.; Yusoh, K.; Ismail, Z. The Preparation of Graphene Ink from the Exfoliation of Graphite in Pullulan, Chitosan and Alginate for Strain-Sensitive Paper. *Int. J. Biol. Macromol.* **2020**, *153*, 1211–1219. [CrossRef]

184. Muth, J.T.; Vogt, D.M.; Truby, R.L.; Mengüç, Y.; Kolesky, D.B.; Wood, R.J.; Lewis, J.A. Embedded 3D Printing of Strain Sensors within Highly Stretchable Elastomers. *Adv. Mater.* **2014**, *26*, 6307–6312. [CrossRef]

185. Shehzad, K.; Shi, T.; Qadir, A.; Wan, X.; Guo, H.; Ali, A.; Xuan, W.; Xu, H.; Gu, Z.; Peng, X.; et al. Designing an Efficient Multimode Environmental Sensor Based on Graphene–Silicon Heterojunction. *Adv. Mater. Technol.* **2017**, *2*, 1600262. [CrossRef]

186. Kim, S.J.; Mondal, S.; Min, B.K.; Choi, C.-G. Highly Sensitive and Flexible Strain–Pressure Sensors with Cracked Paddy-Shaped MoS_2/Graphene Foam/Ecoflex Hybrid Nanostructures. *ACS Appl. Mater. Interfaces* **2018**, *10*, 36377–36384. [CrossRef]

187. Bae, G.Y.; Han, J.T.; Lee, G.; Lee, S.; Kim, S.W.; Park, S.; Kwon, J.; Jung, S.; Cho, K. Pressure/Temperature Sensing Bimodal Electronic Skin with Stimulus Discriminability and Linear Sensitivity. *Adv. Mater.* **2018**, *30*, 1803388. [CrossRef]

188. Abodurexiti, A.; Yang, C.; Maimaitiyiming, X. High-Performance Flexible Pressure and Temperature Sensors with Complex Leather Structure. *Macro Mater. Eng.* **2020**, *305*, 2000181. [CrossRef]

189. Chani, M.T.S.; Karimov, K.S.; Asiri, A.M. Impedimetric Humidity and Temperature Sensing Properties of the Graphene–Carbon Nanotubes–Silicone Adhesive Nanocomposite. *J. Mater. Sci. Mater. Electron.* **2019**, *30*, 6419–6429. [CrossRef]

190. Gao, Z.; Lou, Z.; Han, W.; Shen, G. A Self-Healable Bifunctional Electronic Skin. *ACS Appl. Mater. Interfaces* **2020**, *12*, 24339–24347. [CrossRef] [PubMed]

191. Yang, C.; Abodurexiti, A.; Maimaitiyiming, X. Flexible Humidity and Pressure Sensors Realized by Molding and Inkjet Printing Processes with Sandwich Structure. *Macro Mater. Eng.* **2020**, *305*, 2000287. [CrossRef]

192. Li, Z.; Huang, J.; Zhou, R.; Chen, Z.; Gao, W.; He, J.; Bao, R.; Pan, C. Temperature Decoupling of a Hydrogel-Based Strain Sensor under a Dynamic Temperature Field. *Adv. Mater. Technol.* **2023**, *8*, 2300404. [CrossRef]

193. Zhang, Z.; Zhang, H.; Zhang, Q.; Zhao, X.; Li, B.; Zang, J.; Zhao, X.; Zhang, T. A Pressure and Temperature Dual-Parameter Sensor Based on a Composite Material for Electronic Wearable Devices. *Micromachines* **2023**, *14*, 690. [CrossRef]

194. Ho, D.H.; Sun, Q.; Kim, S.Y.; Han, J.T.; Kim, D.H.; Cho, J.H. Stretchable and Multimodal All Graphene Electronic Skin. *Adv. Mater.* **2016**, *28*, 2601–2608. [CrossRef]

195. Zhuo, H.; Hu, Y.; Tong, X.; Chen, Z.; Zhong, L.; Lai, H.; Liu, L.; Jing, S.; Liu, Q.; Liu, C.; et al. A Supercompressible, Elastic, and Bendable Carbon Aerogel with Ultrasensitive Detection Limits for Compression Strain, Pressure, and Bending Angle. *Adv. Mater.* **2018**, *30*, 1706705. [CrossRef]

196. Qi, Z.; Bian, H.; Yang, Y.; Nie, N.; Wang, F. Graphene/Glycerin Solution-Based Multifunctional Stretchable Strain Sensor with Ultra-High Stretchability, Stability, and Sensitivity. *Nanomaterials* **2019**, *9*, 617. [CrossRef]

197. Park, H.; Kim, J.W.; Hong, S.Y.; Lee, G.; Kim, D.S.; Oh, J.H.; Jin, S.W.; Jeong, Y.R.; Oh, S.Y.; Yun, J.Y.; et al. Microporous Polypyrrole-Coated Graphene Foam for High-Performance Multifunctional Sensors and Flexible Supercapacitors. *Adv. Funct. Mater.* **2018**, *28*, 1707013. [CrossRef]

198. Wang, H.; Tao, J.; Jin, K.; Wang, X.; Dong, Y. Multifunctional Pressure/Temperature/Bending Sensor Made of Carbon Fibre-Multiwall Carbon Nanotubes for Artificial Electronic Application. *Compos. Part A Appl. Sci. Manuf.* **2022**, *154*, 106796. [CrossRef]

199. Qi, K.; He, J.; Wang, H.; Zhou, Y.; You, X.; Nan, N.; Shao, W.; Wang, L.; Ding, B.; Cui, S. A Highly Stretchable Nanofiber-Based Electronic Skin with Pressure-, Strain-, and Flexion-Sensitive Properties for Health and Motion Monitoring. *ACS Appl. Mater. Interfaces* **2017**, *9*, 42951–42960. [CrossRef] [PubMed]

200. Sun, K.; Ko, H.; Park, H.; Seong, M.; Lee, S.; Yi, H.; Park, H.W.; Kim, T.; Pang, C.; Jeong, H.E. Hybrid Architectures of Heterogeneous Carbon Nanotube Composite Microstructures Enable Multiaxial Strain Perception with High Sensitivity and Ultrabroad Sensing Range. *Small* **2018**, *14*, 1803411. [CrossRef]

201. Wang, Y.; Wang, H.; Wang, H.; Zhang, M.; Liang, X.; Xia, K.; Zhang, Y. Calcium Gluconate Derived Carbon Nanosheet Intrinsically Decorated with Nanopapillae for Multifunctional Printed Flexible Electronics. *ACS Appl. Mater. Interfaces* **2019**, *11*, 20272–20280. [CrossRef]

202. Zu, G.; Kanamori, K.; Nakanishi, K.; Huang, J. Superhydrophobic Ultraflexible Triple-Network Graphene/Polyorganosiloxane Aerogels for a High-Performance Multifunctional Temperature/Strain/Pressure Sensing Array. *Chem. Mater.* **2019**, *31*, 6276–6285. [CrossRef]

203. Li, C.; Yang, S.; Guo, Y.; Huang, H.; Chen, H.; Zuo, X.; Fan, Z.; Liang, H.; Pan, L. Flexible, Multi-Functional Sensor Based on All-Carbon Sensing Medium with Low Coupling for Ultrahigh-Performance Strain, Temperature and Humidity Sensing. *Chem. Eng. J.* **2021**, *426*, 130364. [CrossRef]

204. Tung, T.T.; Tran, M.T.; Pereira, A.L.C.; Cordeiro, C.M.B.; Nguyen, D.D.; Tai, N.-H.; Tran, V.V.; Hsu, C.-C.; Joshi, P.; Yoshimura, M.; et al. Graphene Woven Fabric-Polydimethylsiloxane Piezoresistive Films for Smart Multi-Stimuli Responses. *Colloids Surf. B Biointerfaces* **2023**, *221*, 112940. [CrossRef]

205. Liu, H.; Xiang, H.; Wang, Y.; Li, Z.; Qian, L.; Li, P.; Ma, Y.; Zhou, H.; Huang, W. A Flexible Multimodal Sensor That Detects Strain, Humidity, Temperature, and Pressure with Carbon Black and Reduced Graphene Oxide Hierarchical Composite on Paper. *ACS Appl. Mater. Interfaces* **2019**, *11*, 40613–40619. [CrossRef]

206. Lee, J.H.; Heo, J.S.; Kim, Y.; Eom, J.; Jung, H.J.; Kim, J.; Kim, I.; Park, H.; Mo, H.S.; Kim, Y.; et al. A Behavior-Learned Cross-Reactive Sensor Matrix for Intelligent Skin Perception. *Adv. Mater.* **2020**, *32*, 2000969. [CrossRef]

207. Wang, X.; Yue, O.; Liu, X.; Hou, M.; Zheng, M. A Novel Bio-Inspired Multi-Functional Collagen Aggregate Based Flexible Sensor with Multi-Layer and Internal 3D Network Structure. *Chem. Eng. J.* **2020**, *392*, 123672. [CrossRef]

208. Zhang, X.; Zhang, G.; Wang, F.; Chi, H. Evolution of Oxygen Content of Graphene Oxide for Humidity Sensing. *Molecules* **2024**, *29*, 3741. [CrossRef] [PubMed]

209. Ali, A.-M.B.H.; Elmasry, M.R.; Bin Jardan, Y.A.; El-Wekil, M.M. Smart Fluorometric Sensing of Metal Contaminants in Canned Foods: A Carbon Dot-Based Dual-Response System for Quantifying Aluminum and Cobalt Ions. *RSC Adv.* **2025**, *15*, 6962–6973. [CrossRef] [PubMed]

210. Bricha, M.; El Mabrouk, K. Effect of Surfactants on the Degree of Dispersion of MWNTs in Ethanol Solvent. *Colloids Surf. A Physicochem. Eng. Asp.* **2019**, *561*, 57–69. [CrossRef]

211. Thines, R.K.; Mubarak, N.M.; Nizamuddin, S.; Sahu, J.N.; Abdullah, E.C.; Ganesan, P. Application Potential of Carbon Nanomaterials in Water and Wastewater Treatment: A Review. *J. Taiwan Inst. Chem. Eng.* **2017**, *72*, 116–133. [CrossRef]

212. Meyer, E.; Bede, A.; Zingwe, N.; Taziwa, R. Metal Sulphides and Their Carbon Supported Composites as Platinum-Free Counter Electrodes in Dye-Sensitized Solar Cells: A Review. *Materials* **2019**, *12*, 1980. [CrossRef]

213. Medrano-Lopez, J.A.; Villalpando, I.; Salazar, M.I.; Torres-Torres, C. Hierarchical Nanobiosensors at the End of the SARS-CoV-2 Pandemic. *Biosensors* **2024**, *14*, 108. [CrossRef]

214. Ariati, R.; Sales, F.; Souza, A.; Lima, R.A.; Ribeiro, J. Polydimethylsiloxane Composites Characterization and Its Applications: A Review. *Polymers* **2021**, *13*, 4258. [CrossRef]

215. Hong, S.; Kim, H.; Qaiser, N.; Baumli, P.; Hwang, B. A Review of Recent Progress in Fabrication Methods and Applications of Polydimethylsiloxane Sponge. *J. Nat. Fibers* **2023**, *20*, 2264497. [CrossRef]

216. Marcuello, C.; Foulon, L.; Chabbert, B.; Aguié-Béghin, V.; Molinari, M. Atomic Force Microscopy Reveals How Relative Humidity Impacts the Young's Modulus of Lignocellulosic Polymers and Their Adhesion with Cellulose Nanocrystals at the Nanoscale. *Int. J. Biol. Macromol.* **2020**, *147*, 1064–1075. [CrossRef]

217. Korotcenkov, G.; Simonenko, N.; Simonenko, E.; Sysoev, V.; Brinzari, V. Paper-Based Humidity Sensors as Promising Flexible Devices, State of the Art, Part 2: Humidity-Sensor Performances. *Nanomaterials* **2023**, *13*, 1381. [CrossRef]

218. Page, M.J.; McKenzie, J.E.; Bossuyt, P.M.; Boutron, I.; Hoffmann, T.C.; Mulrow, C.D.; Shamseer, L.; Tetzlaff, J.M.; Akl, E.A.; Brennan, S.E.; et al. The PRISMA 2020 statement: An updated guideline for reporting systematic reviews. *BMJ* **2021**, *372*, n71. [CrossRef]